

Automating Vehicles by Deep Reinforcement Learning using Task Separation with Hill Climbing

Mogens Graf Plessen

Abstract—Within the context of autonomous vehicles, classical model-based control methods suffer from the trade-off between model complexity and computational burden required for the online solution of expensive optimization or search problems at every short sampling time. These methods include sampling-based algorithms, lattice-based algorithms and algorithms based on model predictive control (MPC). Recently, end-to-end trained deep neural networks were proposed to map camera images directly to steering control. These algorithms, however, a priori dismiss decades of vehicle dynamics modeling experience, which could be leveraged for control design.

In this paper, a model-based reinforcement learning (RL) method is proposed for the training of feedforward controllers in the context of autonomous driving. Fundamental philosophy is to offline train on arbitrarily sophisticated models, while online cheaply evaluate a feedforward controller, thereby avoiding the need for online optimization. The contributions are, first, the discussion of two closed-loop control architectures, and, second, the proposition of a simple gradient-free algorithm for deep reinforcement learning using task separation with hill climbing (TSHC). Therefore, a) simultaneous training on separate deterministic tasks with the purpose of encoding motion primitives in a neural network, and b) the employment of maximally sparse rewards in combinations with virtual actuator constraints on velocity in setpoint proximity are advocated. For feedforward controller parametrization, both fully connected (FC) and recurrent neural networks (RNNs) are used.

Index Terms—Automated Vehicles, Deep Reinforcement Learning, Continuous Control, Hill Climbing, Sparse Rewards

I. INTRODUCTION

There exists a plethora of motion planning and control techniques for self-driving vehicles [1]. The diversity is caused by a core difficulty: the trade-off between model complexity and permitted online computation at short sampling times. Let us briefly review three popular control classes for automated vehicles, recent end-to-end solutions, before summarizing the motivation and contribution of this paper.

A. Model-based control methods

In [2], a *sampling-based* anytime algorithm RRT* is discussed. Key notion is to *refine* an initial suboptimal path *while* it is followed. As demonstrated, this is feasible when driving towards a static goal in a static environment. However, it may be problematic in dynamic environments requiring to constantly replan paths, and where an online sampled suitable trajectory may not be returned in time. Other problems of *on-line* sampling-based methods are a limited model complexity and their tendency to produce jagged controls that require a smoothing step, e.g., via conjugate gradient [3].

In [4], a *lattice-based* method is discussed. Such methods, and similarly also based on *motion primitives* [5], [6], [7], [8], are always limited by the size of the look-up table that can be searched in real-time. In [4], a GPU is used for search.

In [9], *linear time-varying model predictive control* (LTV MPC) is discussed for autonomous vehicles. While appealing for its ability to incorporate constraints, MPC must trade-off model-complexity vs. computational burden from solving optimization problems online. Furthermore, MPC is dependent on state and input reference trajectories, at least for linearization of dynamics, but almost always also for providing a tracking reference. Therefore, a two-layered approach is often applied, with motion planning and tracking as the two layers [1]. See [10] for a method using geometric corridor planning in the first layer for reference generation and for the combinatorial decision taking on which side to overtake obstacles. As indicated in [9, Sect. V-A] and further emphasized in [11], the selection of reference velocities can become problematic for *time-based* MPC and motivated to use *spatial-based* system modeling. Vehicle dynamics can be incorporated by inflating obstacles [7]. For tight maneuvering, a linearization approach [12] is more accurate, however, computationally more expensive.

To summarize, two core observations are made. First, all methods (from sampling-based to MPC) are derived from vehicle *models*. Second, all of above methods suffer from the real-time requirement of short sampling times. As a consequence, all methods make simplifications on the employed model. These include, for example, omitting of dynamical effects, tire dynamics, vehicle dimensions, using inflated obstacles, pruning search graphs, solving optimization problems iteratively, or offline precomputing trajectories.

B. Vision-based methods

In [13], a pioneering end-to-end trained neural network labeled ALVINN was used for steering control of an autonomous vehicle. Video and range measurements are fed to a *fully connected* (FC)-network with a single hidden layer with 29 hidden units, and an output layer with 45 direction output units, i.e., *discretized* steering angles, plus one road intensity feedback unit. ALVINN does not control velocity and is trained using supervised learning based on road “snapshots”. Similarly, recent DAVE-2 [14] also only controls steering and is trained supervisedly. However, it outputs *continuous* steering action and is composed of a network including *convolutional neural networks* (CNN) as well as FC-layers with a total of 250000 parameters. During testing (i.e., after training), steering commands are generated from *only* a front-facing camera. Another end-to-end system based on only camera vision is

presented in [15]. First, a driving intention (change to left lane, change to right lane, stay in lane and break) is determined, before steering angle is output from a *recurrent neural network* (RNN). Instead of mapping images to steering control, in [16] and [17], *affordance indicators* (such as distance to cars in current and adjacent lanes etc.) and feasible driving actions (such as straight, stop, left-turn, right-turn) are output from neural networks, respectively. See also [18] and their treatment of “option policies”. To summarize, it is distinguished between a) vision-based *end-to-end* control, and b) *perception-driven* approaches that attempt to extract useful features from images. Note that such features (e.g., obstacle positions) are implicitly required for all methods from Section I-A.

C. Motivation and Contribution

This work is motivated by the following considerations. As noted in [19], correct localization relative to lane boundaries is more important than with respect to GPS-coordinates. This indicates the importance of lasers, lidars and cameras for automated driving. Second, vehicles are man- and woman-made products for which there exist decade-long experience in vehicle dynamics modeling [20],[21]. There is no sensible reason to a priori entirely discard this knowledge (for manufacturers it is present even in form of construction plans). Thus, available vehicle models should be leveraged for control design. Consider also the position paper [22] for general limitations of end-to-end learning. Third, a general purpose control setup is sought avoiding to switch between different vehicle models and algorithms for, e.g., highway driving and parking. There also exists only one real-world vehicle. In that perspective, the most complex vehicle model encompassing all driving scenarios is in general preferable for control design. Also, a model mismatch on the planning and tracking layer can incur paths infeasible to track [7]. Fourth, the most accident causes involving other mobile vehicles are *rear-end* collisions [23], which most frequently are caused by inattentiveness or too close following distances. In [10] it was found that reaction delays of a single sampling time can already decide upon crash avoidance or failure. Therefore, a control method that enables minimal sampling times, such as feedforward control, can significantly increase safety. Importantly, this is achieved deterministically. In contrast, environment motion prediction (which also can increase safety) always remains stochastic. Fifth, small sampling times are contradicting the preference for complex vehicle models. These considerations motivate to use *neural network controllers*, which enable:

- 1) *Offline* training on arbitrarily sophisticated high-fidelity models in arbitrarily complex simulation environments.
- 2) *Online* fast network feedforward evaluation.

Because of these two characteristics, neural network controllers have the potential to eventually also be employed in nano-scale robots [24]. In an automated vehicles settings, it implies that once trained, low-cost embedded hardware can be used online with only a few matrix vector multiplications being evaluated forward.

The contribution is as follows. First, out of two candidates, a suitable closed-loop control architecture for general purpose driving based on neural networks is identified. Second, a

simple gradient-free algorithm for model-based deep reinforcement learning using task separation with hill climbing (TSHC) is presented. It is proposed to a) simultaneously train on separate deterministic tasks with the purpose of encoding motion primitives in a neural network, and b) during training to employ maximally sparse rewards in combinations with virtual actuator constraints on velocity in setpoint proximity. Both fully connected (FC) and recurrent neural networks (RNNs) are used for feedforward controller parametrization.

The remainder of this paper is organized as follows. After a motivational example, the problem is formulated in Section III. In Section IV two closed-loop architectures are discussed. The main algorithm TSHC is presented in Section V. Numerical experiments are discussed in Section VI, before concluding.

II. MOTIVATING EXAMPLE

Let us consider an exemplary freeform navigation task, see Fig. 1. Extending previous work, one solution approach is to use *sequential convex optimization* (SCP) as follows:

- 1) Dismissing the obstacles at first, connect the vehicle start and end pose by a piecewise-affine (PWA) trajectory.
- 2) Use the PWA trajectory as a reference for a LTV-MPC tracking controller.
- 3) Use the LTV-MPC trajectory as the “road centerline” in a spatial-based MPC-framework, mapping obstacles, planning a corridor [10], and accounting for vehicle dimensions in a road-aligned coordinate frame [12].

Several remarks can be made. First, the heuristic for PWA trajectory generation is largely shaping the overall result. For above example, basic notion is to alternately generate rays starting from the end and start vehicle pose, avoiding intersections in start and end positions to encourage outreaching steering behavior, and turning perpendicularly after, for example, 5m (or the minimum velocity-dependent turning radius) either always counterclockwise (CCW) or always clockwise (CW) if no intersection is yet reached. In Fig. 1, the CW-solution is displayed. This heuristic can be extended by *intermediate locations* when admitting changes of velocity sign. Second, as demonstrated the method successfully permits tight maneuvering. In general, a LTV-MPC tracking controller based on the nonlinear kinematic bicycle model [21] was found to be very robust even when tracking edgy paths. Since LTV-MPC is time-parameterized and thus heavily dependent on reference velocity, constraint formulation for obstacle avoidance is problematic [11]. This is the reason for the subsequent *spatial*-based MPC. Then, its trajectory output is used as reference for a *second* spatial-based MPC, which generates a further smoothed trajectory, and permits to use friction constraints and also time-scheduling [11]. Despite tight obstacle avoidance, several limitations are obvious. First, there are small wiggles (including a decrease in output velocity) in the final trajectory resulting from the very large deviations between LTV-MPC reference and final trajectory (after linearization and accounting for obstacles). Second, the dependence on reference trajectories is apparent. Third, the computational complexity associated with three sequential MPCs is high.

This implies a) employment of a simplified vehicle model and b) limitedly small sampling times, which both negatively

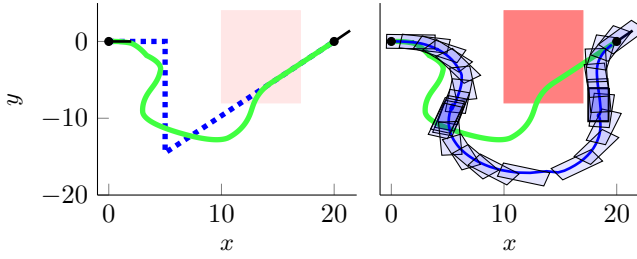


Fig. 1. Motivating example: a freeform navigation task with one obstacle. A trajectory is sought connecting the two black indicators, avoiding the red obstacle and accounting for vehicle dimensions. (Left) Dismissing the obstacle, the heuristic PWA trajectory (blue dotted) and LTV-MPC tracking result (green) are shown. (Right) The final trajectory after two iterations of spatial-based MPC with linearized vehicle dynamics. A hybrid of [12] and [11] is used with the time-optimal smooth-steering objective from the latter reference. In contrast to *rectangle-envelopes* aligned with the road-centerline in [12], obstacle contours are mapped directly and without any margins. This enables maximally tight maneuvering.

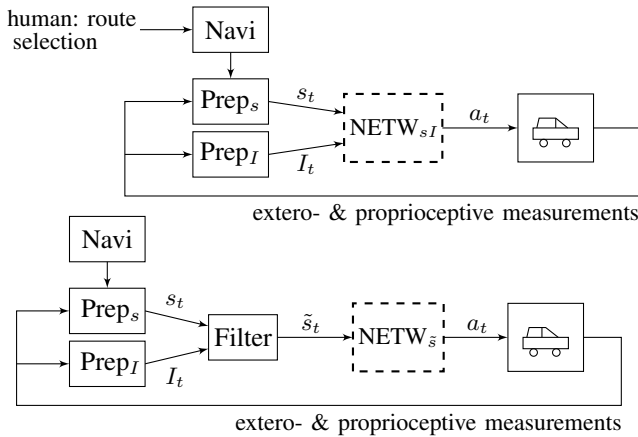


Fig. 2. Two candidates for the closed-loop control system architecture.

affect safety. This example is given to illustrate a need for fast motion planning algorithms that can leverage high-fidelity nonlinear vehicle models to plan trajectories between any two locations in space and accounting for vehicle dimensions.

III. PROBLEM FORMULATION

Let vector $z_t = [x_t, y_t, \psi_t, v_t]$ summarize four of the vehicle’s states. Coordinates x_t and y_t describe the center of gravity (CoG) in the inertial frame, ψ_t denotes the yaw angle relative to the inertial frame, and v_t indicates the vehicle’s speed at time t . Let $z^{\text{goal}} = [x^{\text{goal}}, y^{\text{goal}}, \psi^{\text{goal}}, v^{\text{goal}}]$ denote a goal state. Then, the following problem can be formulated.

Problem 1. *Given vector z_t at time t , determine a general purpose control method that enables closed-loop navigation from z_t to z^{goal} , accounting for physical actuator constraints, and ensuring obstacle avoidance.*

Thus, a general purpose control method that can serve the entire range of driving operations is sought. These include road following (RF), intersection control (IC), static and dynamic obstacle avoidance (OA), adaptive cruise control (ACC) and parking applications. Four main classes are distinguished:

- Zone navigation (no obstacles, no road bounds);
- Road navigation (static obstacles, road bounds);

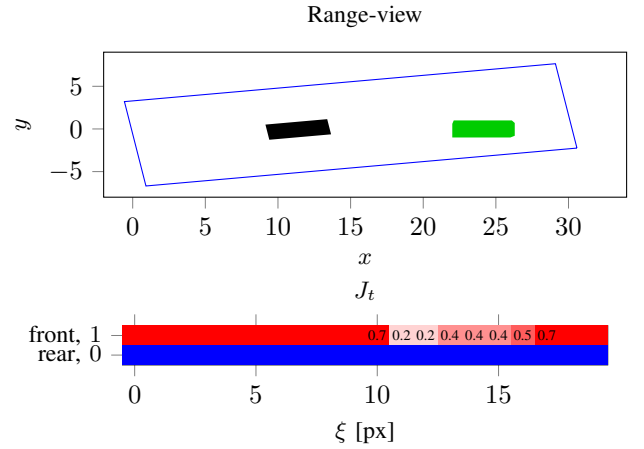


Fig. 3. (Top) Illustration of the range-view concept. Black indicates the ego vehicle and green a detected obstacle. (Bottom) Illustration of $J_t \in \mathbb{R}^{2 \times N_\epsilon}$ with matrix entries normalized along the length (longer rectangle edge) of the range-view. Colors are displayed for emphasis.

- Adaptive cruise control (ACC) on top of road navigation;
- Dynamic obstacle avoidance on top of road navigation.

The choice of four-state z_t is motivated by this distinction, since instances of all four classes can be characterized by an associated z^{goal} and a deviation measure relating z_t to z^{goal} . In addition, z^{goal} can be reassigned recursively such that it is rendered *time-varying* z_t^{goal} . This enables to encode IC as well as ACC applications.

IV. SYSTEM LEVEL

A. Closed-loop control system

Two candidate architectures are considered, see Fig. 2. Besides the vehicle to be controlled, there are four core components common to both. The first is a neural network acting as the controller, abbreviated as “NETW” and subscripted by \bar{s} and s_I , respectively. They differ by their input vector. Thus,

$$s_t = \{z_\tau - z_\tau^{\text{goal}}\}_{\tau=t-\Gamma}^t, \quad (1)$$

$$I_t = \{J_\tau\}_{\tau=t-\Gamma}^t, \quad (2)$$

are defined, where hyperparameter $\Gamma \geq 0$ denotes the number of past states considered, and where J_τ is a pixel-related multi-dimensional array that is further motivated in Section IV-C. In the general case, z_τ^{goal} is time-varying. However, for e.g. parking applications, it is static $z_\tau^{\text{goal}} = z^{\text{goal}}, \forall \tau$. “Filter” denotes an algebraic mapping from (s_t, I_t) to \tilde{s}_t . For example, in the simplest case, $\tilde{s}_t = s_t$. The block output of NETW is a control signal a_t , further described in Section IV-D. The entire Section V is devoted to the design and training of NETW. The second component in Fig. 2 is “Navi” (navigation planner). It outputs a high-level route plan. The third and fourth block component are labeled as “Prep_s” and “Prep_I” since they receive extero- and proprioceptive sensor measurements, process these, and prepare them (hence abbreviation “Prep”) such that s_t and I_t according to (1) and (2) can be fed to the control network. Exteroceptive measurements are assumed to include inter-vehicular communication (car-2-car) sensings as well as the communication with a centralized

or decentralized coordination service such that, in general, multi-automated vehicle coordination is also enabled [25].

B. Location, heading and velocity-related system component

The choice of s_t in (1) is discussed. Nonlinear dynamic vehicle models that include tire dynamics can be very complex with up to a double-digit number of states [21]. For all kinematic and dynamic vehicle models, and of varying complexity, the goal vehicle pose, within a time-varying and a static setting, can be described well by only location, heading and velocity, i.e., $z_\tau^{\text{goal}} = [x_\tau^{\text{goal}}, y_\tau^{\text{goal}}, \psi_\tau^{\text{goal}}, v_\tau^{\text{goal}}]$. This entails the question of what to provide as input to the network controller: a high-dimensional state according to the vehicle model used for training, or only a four-dimensional $z_\tau = [x_\tau, y_\tau, \psi_\tau, v_\tau]$. It is opted for the latter option. This is motivated as follows. Because of receiving reward measures as a function of z_τ^{goal} during training, the network controller naturally encodes vehicle dynamics when mapping s_t and I_t (or \tilde{s}_t) to a_t . It is not obvious how providing a more detailed state (e.g., including various *rate* states) as input to the network would improve this encoding since the goal pose can already be described accurately by the only four-dimensional z_τ^{goal} .

C. Pixel-related system component

This section discusses I_t in (2). It is proposed to map all exteroceptive measurements to *one sparse multi-channel* image. One of these channels describes all area prohibited from trespassing (obstacles) within a *range-view* in the proximity of the vehicle, see Fig. 3. This permits general purpose driving according to the four classes described in Section III. This approach also exploits the fact that vehicles operate ground-based. Thus, for all obstacle avoidance tasks the area prohibited from trespassing can be described accurately in the 2D plane. Image-sparsity naturally results from the distinction between area permitted (pixel-value zero) and area prohibited to drive in (pixel value greater than zero). It also permits to distinguish between obstacles of different kind (static, dynamic, bicycles, vehicles etc.) by assigning different pixel values. Third, a sparse multi-channel image is a well-suited input for training of *location-aware* neural networks (such as fully connected ones). Fourth, it guarantees a fixed-size complexity of I_t (fixed pixel resolution) fed to the neural network controller, while at the same time permitting an adaptable, e.g., velocity-dependent range-view size. Thus, complexity is always bounded by the number of pixels, $N_\eta \times N_\xi$, employed to represent the range-view.

In addition, a simplification of the sparse multi-channel image is considered. The first layer of the I_t -related part of the network controller (NETW) receives an input vector of dimension $N_I = (1 + \Gamma)N_c N_\xi N_\eta$. Dependent on the image resolution and since typically $N_\eta > N_\xi$, the number N_I can be quite large. Therefore, an alternative I_t is proposed, where each image-frame, $\tilde{J}_{\tau,c} \in \mathbb{R}^{N_\eta \times N_\xi}$, is replaced by a reduced $J_{\tau,c} \in \mathbb{R}^{2 \times N_\xi}$ array. Thus, it is defined

$$J_{\tau,c,1,\xi} = \arg \min_{\eta} \left\{ \tilde{J}_{\tau,c,\eta,\xi} > 0 \right\}_{\eta=N_\xi^{\text{CoG}}}^{N_\eta} - K_\xi^{\text{max}}, \quad (3a)$$

$$J_{\tau,c,0,\xi} = -K_\xi^{\text{min}} + \arg \max_{\eta} \left\{ \tilde{J}_{\tau,c,\eta,\xi} > 0 \right\}_{\eta=0}^{N_\xi^{\text{CoG}}}, \quad (3b)$$

with $K_\xi^{\text{max}} = \max(N_\xi^{\text{CoG}}, N_\xi^{\text{veh,max}})$ and $K_\xi^{\text{min}} = \min(N_\xi^{\text{CoG}}, N_\xi^{\text{veh,min}})$ for all $\tau = t - \Gamma, \dots, t$, $c = 1, \dots, N_c$, $\xi = 0, \dots, N_\xi - 1$. Thus, the signed minimum pixel distances between vehicle chassis, $N_\xi^{\text{veh,max}}$ and $N_\xi^{\text{veh,min}}$, or CoG, N_ξ^{CoG} , and closest obstacle in forward and backward facing directions are represented, see Fig. 3. The multi-channel description is maintained, such that, one channel can describe distance, while another the obstacle-type (static, dynamic, etc.) or road surface. It is further argued that network learning capability is *not* affected when enabling *temporal* data processing (i.e., with memory). This can be seen when envisioning how the network controller can learn to pass by obstacle corners. Temporal perception processing enables to learn anticipative and, in particular, outreaching steering. This motivates that either a) *multilayer perceptrons* (MLPs) with $\Gamma > 0$ are employed, or, b) and alternatively, recurrent neural networks (RNNs).

The sensor fusion of all exteroceptive measurements in order to obtain a unified I_t -array is the second main task besides design of a learning algorithm to train the network. It includes a transformation step from various physical measurement units to pixel-coordinates. See [26] for *semantic segmentation* based on *fully convolutional networks* (FCN). Importantly, note that a) sensor fusion to obtain I_t , and b) the training of the network controller can be solved *orthogonally*. The former problem is of *supervised* machine learning nature. In contrast, the latter represents a *reinforcement learning* problem to which the entire Section V is devoted to.

D. Control vector

The *continuous* control vector is defined as

$$a_t = [v_t, \delta_t]. \quad (4)$$

Both v_t and δ_t are subject to physical actuator absolute and rate constraints. These are treated as *part of the vehicle model* on which the network training is based on (see the next Section). Note that the minimum velocity is negative. Hence, reverse driving is explicitly permitted. The network output, which results from a $\tanh(\cdot)$ activation function as will be further specified below, is linearly scaled to be within *absolute* actuator bounds, before it is fed to the low-level controllers that are further limited by actuator *rate* constraints.

A remark with respect to gear selection can be made. Throughout this paper, electric vehicles (EVs) are assumed since they appear more suitable to curb urban pollution. EVs do not require gearboxes. Nevertheless, the network architecture can be extended to include discrete gear as an additional decision variable. Suppose N_{gears} gears are available. Then, the output layer can be extended by N_{gears} channels, with each channel output representing a normalized probability of gear selection as a function of s_t and I_t (or \tilde{s}_t), that can be trained by means of a *softmax classifier*.

In fact, the last discussion further underlines the potential of model-based reinforcement learning using neural networks. Similarly, *mixed-integer* decisions such as on which side to overtake an obstacle at what speed can in principle be handled efficiently using the neural approach.

E. Exemplary system model used for learning

A fundamental motivation of proposed method is to leverage decade-long experience in vehicle modeling [20], [21]. Since vehicles are man- and woman-made products, there is no sensible reason to discard existing vehicle model equations and construction insights. For reduced computational burden in this proof of concept, a simple nonlinear bicycle model is employed for the experiments in Section VI. Note, however, that in practice it is recommended to employ a high-fidelity vehicle model. Physical actuator absolute and rate constraints are treated as part of the vehicle model on which the network training is based on. The deterministic system model assumes

$$v_t \leq \min(v_t, v_{t-1} + \dot{v}_{\max,t} T_s, \tilde{I}_{v,t-1}^{\max} v_{\max,t}) \quad (5a)$$

$$v_t \geq \max(v_t, v_{t-1} + \dot{v}_{\min,t} T_s, \tilde{I}_{v,t-1}^{\min} v_{\max,t}) \quad (5b)$$

with $\tilde{I}_{v,t-1}^{\max} = 1$ if $v_{t-1} \geq 0$ and 0 otherwise, and $\tilde{I}_{v,t-1}^{\min} = 1$ if $v_{t-1} \leq 0$ and 0 otherwise. The two indicators are introduced to guarantee a zero-crossing w.r.t. v -control to remain for at least one T_s at zero velocity. Furthermore, there is $\delta_t \leq \min(\delta_t, \delta_{t-1} + \dot{\delta}_{\max,t} T_s, \delta_{\max,t})$, $\delta_t \geq \max(\delta_t, \delta_{t-1} + \dot{\delta}_{\min,t} T_s, \delta_{\max,t})$, and a simple Euler-discretized nonlinear kinematic bicycle model with $x_{t+1} = x_t + T_s v_t \cos(\psi_t)$, $y_{t+1} = y_t + T_s v_t \sin(\psi_t)$, $\psi_{t+1} = \psi_t + T_s \frac{v_t}{l_f} \tan(\delta_t)$, $v_{t+1} = v_t$, modeled with $l_f = 3.5\text{m}$, and rectangular vehicle dimensions of $1.8 \times 4.3\text{m}$.

F. General purpose method

At mission initialization, a navigation route is computed. Then, the following basic algorithm can be conducted:

- 1) Determine (z_t, I_t) from a mapping of proprio- and exteroceptive sensors to account for road boundaries, static and dynamic obstacles, traffic lights and signs.
- 2) Determine $f_t^{\text{ACC}} \in \{0, 1\}$, a flag for ACC-possibility.
- 3) If $f_t^{\text{ACC}} == 1$, then apply conservative driving with

$$z_t^{\text{goal}} = \begin{cases} z_t^{\text{stop}}, & \text{if } \exists \text{ red traffic light/sign ahead,} \\ z_t^{\text{lead}}, & \text{if } d_t < d^{\min}(v_t, v_t^{\text{lead}}), \\ z_t^{\text{horizon}}, & \text{otherwise,} \end{cases}$$

otherwise apply emergency obstacle avoidance with $z_t^{\text{goal}} = z_t^{\text{distant}}$ and *relaxed* permissible driving area.

- 4) Evaluate NETW as a function of s_t and I_t to obtain a_t .
- 5) Apply a_t and wait until the next sampling time.

Thus, three parameterized *decisions* need to be made. First, on the possibility of ACC. This decision can typically be parameterized as a function of current and leading vehicle state. The second decision is about a still tolerable minimum safety distance $d_t < d^{\min}(v_t, v_t^{\text{lead}})$ with respect to a leading vehicle characterized by state z_t^{lead} . See [10] for a simple heuristical parameterization of both of the first two decisions. The third decision involves a selection of a suitable goal state in case of an emergency obstacle avoidance scenario. Therefore, a vehicle state z_t^{distant} located *distant* away but along the reference path may heuristically be imposed. This permits the control system to fully concentrate on immediate obstacle avoidance rather than tracking of a reference state.

Relaxation of permissible driving area implies to also consider neighboring lanes for a potential obstacle avoidance maneuver. In contrast to above heuristic decisions, z_t^{stop} with $v_t^{\text{stop}} = 0$ is prescribed by traffic lights and stop signals. For road tracking, the goal state is set as z_t^{horizon} , i.e., the intersection of the navigation route and the range-view.

G. Discussion and comparison with model predictive control

Before presenting the learning algorithm, main differences to MPC are stressed. First, implicit MPC solves an optimization problem *online*. This limits the complexity of the predictive models that can be used. In contrast, neural network controllers can be trained offline on the most sophisticated vehicle models, before being employed online in a computationally cheap feedforward evaluation. As a consequence, online solvers for MPC are not required anymore.

Second, it is also mentioned *explicit* MPC [27], which reduces online burden to search in a look-up table as a function of current state (MPC problems are parameterized as a function of state and solved offline). Explicit MPC is limited to a) *time-invariant* models (and thus unsuited for general navigation tasks), b) still requires an online search of the look-up table storing the state-dependent controls, and c) only suitable for small problems. For perspective, in [28] for problems with more than approximately 5 states, 3 controls and 12 inequality constraints, explicit MPC is considered to no longer be practically feasible. It may be interesting to analyze that simple explicit (linear) MPC applications can be replaced by neural network feedforward controllers, which are a) trained on more complex (nonlinear) system models using reinforcement learning and b) are still faster to evaluate online.

Third, spatial-based MPC can be superior to time-based MPC due to its ability to easily constrain vehicle motion to a convex driving corridor expressed along a spatially discretized road centerline. In proposed neural network setting, this driving corridor is represented by a pixel image. Importantly and in contrast to MPC, convexity of permissible driving area is not a prerequisite anymore. This, in general, liberates from the convex corridor planning step preceding MPC, see [10] and the references therein.

Fourth, while MPC optimizes over a *predictive* model, the nature of neural network controllers appears of more *reactive* nature, eventhough predictive capability is encoded in the network through training and receding z_t^{goal} -selection during online operation. The most frequent accident cause involving other mobile vehicles are *rear-end* collisions [23], which most frequently result from inattentiveness or too close following distances. In this perspective, another interesting topic is to argue to what extend *fast reaction* times are more important in automated vehicles than predictive capability.

Finally, in view of current (and further developing) hardware opportunities, expensive offline training clearly is appropriate. To stress remarkable dimensions, in [29] training is distributed on 80 machines and 1440 CPU cores. Even more remarkable, in [30] 1024 Tesla P100 GPUs are used in parallel. For perspective, one Tesla P100 permits a double-precision performance of 4.7 TeraFLOPs [31].

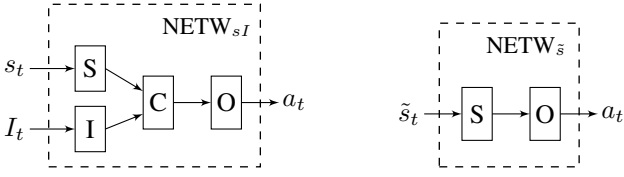


Fig. 4. The two network structures of the control block candidates in Fig. 2. It is distinguished between a S (s_t/\tilde{s}_t -related), I (I_t -related), C (combined) and O (output layer) part of the neural network. Each of the four parts can be composed of an arbitrary sequence of FCs and RNNs.

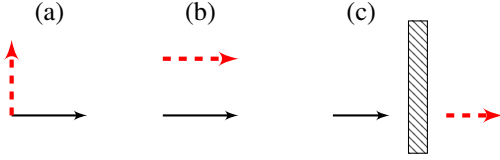


Fig. 5. The problematic of rich rewards. Three scenarios (a), (b) and (c) indicating different start (black) and goal (red dashed) states (position and heading). For (c), an obstacle is added.

V. TRAINING ALGORITHM

This section proposes a simple learning method to train the neural network controller in Fig. 2.

A. Network controller

Two network structure candidates are displayed in Fig. 4. Alternative structures were also tested, but did not improve performance, or only increased the total number of weights to be learnt (e.g., when decoupling controls and not sharing weights). Each of the four parts displayed in Fig. 4 can be composed of an arbitrary sequence of FCs, LSTM cells including peephole connections [32],[33], and GRUs [34]. Motivation for these choices are the simplicity of FCs and the temporal processing ability of RNNs. All parameter weights to be learnt are initialized by Gaussian-distributed variables with zero mean and a small variance σ_{init}^2 . Exceptions are adding a 1 to the LSTMs forget gate biases for LSTM cells, as recommended in [35], which are thus initialized with mean 1. In proposed setting, the affine part of all FC-layers is followed by nonlinear $\tanh(\cdot)$ activation functions acting elementwise. Because of their bounded outputs, saturating nonlinearities are preferred over ReLUs, which are used for the hidden layers in other RL settings [36] but can result in large unbounded layer output changes. Before entering the first layers of the S- and I-block, s_t and I_t are normalized elementwise, whereby for final experiments 30m , 2π , $v_{\text{max}} - v_{\text{min}}$ and N_η are heuristically selected as normalization constants for distances x_t and y_t , angle ψ_t , velocity v_t and all elements of I_t , respectively. Their choice was not found to be decisive for learning. The final FC-layer comprises a $\tanh(\cdot)$ activation function. It accordingly outputs two bounded continuous values referred to as a_t^{NN} , which are then affinely scaled to a_t as outlined in the next section. Then, during training a_t is fed to the system model from Section IV-E.

B. Reward shaping

Reward shaping is crucial for the success of learning by reinforcement signals [37]. However, it was found to be a

highly delicate matter in practical problems. Therefore, the preferred choice is motivated in detail.

In most practical control problems, a current state z_0 is given at $t = 0$, and a desired goal state z^{goal} is known. Not known, however, is the shape of the best trajectory (w.r.t. a given criterion) and the control signals that realize that trajectory. Thus, by nature these problems offer a *sparse* reward signal, $r_{\tilde{T}}(z^{\text{goal}})$, received only upon reaching the desired goal state at some time $\tilde{T} > 0$. In the following, auxiliary *rich* reward signals and *curriculum learning* [38] are first discussed.

A reward signal $r_t(z_t, a_t)$, abbreviated by r_t , is labeled as *rich* when it is *time-varying* as a function of states or controls. Note that the design of any such signal is heuristic and motivated by the hope for accelerated learning through maximally frequent feedback. In the following, the problematic of rich rewards is exposed. First, $e_{d,t} = \sqrt{(x_t - x^{\text{goal}})^2 + (y_t - y^{\text{goal}})^2}$, $e_{\psi,t} = |\psi_t - \psi^{\text{goal}}|$, $e_{v,t} = |v_t - v^{\text{goal}}|$ are defined, as well as the binary flag indicating whether the goal state is reached

$$f_t^{\text{goal}} = \begin{cases} 1, & \text{if } (e_{d,t} < \epsilon_d) \wedge (e_{\psi,t} < \epsilon_\psi) \wedge (e_{v,t} < \epsilon_v), \\ 0, & \text{otherwise,} \end{cases} \quad (6)$$

where $(\epsilon_d, \epsilon_\psi, \epsilon_v)$ are small tolerance hyperparameters. Then, suppose a rich reward signal of the form $r_t = -(\alpha e_{d,t} + e_{\psi,t})$ is designed, which characterizes a weighted linear combination of different measures. This class of reward signals, trading-off various terms and providing feedback at every step, occurs frequently in the literature [39], [40], [36], [41]. However, as will be shown, in an automotive setting, it may easily lead to undesirable behavior. Suppose case (a) in Fig. 5 and a maximum simulation time T^{max} . Then, omitting a discount factor for brevity, $-T^{\text{max}} \frac{\pi}{2} > -\sum_{t=0}^{\tilde{T}} \alpha e_{d,t}^* + e_{\psi,t}^*$, may be obtained for accumulated rewards. Thus, the no-movement solution may incur more accumulated reward, namely $-T^{\text{max}} \frac{\pi}{2}$, in comparison to the true solution, which is indicated on the right-hand side of the inequality sign.

Similarly, for specific (α, T^{max}) , the second scenario (b) in Fig. 5 can return a no-movement solution since the initial angle is already coinciding with the target angle. Hence, for a specific (α, T^{max}) -combination, the accumulated reward when not moving may exceed the value of the actual solution.

The third scenario (c) in Fig. 5 further illustrates that even if reducing rich rewards to a single measure, e.g., $r_t = -e_{d,t}$, an undesired standstill may result. This occurs especially in the presence of obstacles (and maze-like situations in general).

To summarize, for finite T^{max} , the design of auxiliary *rich* reward signals is not straightforward. It can easily result in solution trajectories that may even be *globally optimal* w.r.t. accumulated reward, however, prohibit to solve the original problem of determining a trajectory from initial to target state.

In [38], curriculum learning (CL) is discussed as a method to speed up learning by providing the learning agent first with *simpler* examples before gradually increasing complexity. Analogies to humans and animals are drawn. The same paper also acknowledges the difficulty of determining “interesting” examples [38, Sect. 7] that optimize learning progress.

Indeed, CL entails the following issues. First, “simpler” tasks need to be identified. This is not straightforward as discussed shortly. Second, these tasks must first be solved



Fig. 6. Curriculum Learning. The difficulty of selecting “simple” examples. The original problem with start (black) and goal (red dashed) state is denoted in (a). A “simpler” problem is given in (b). See Section V-B for interpretation.

before their result can serve as initialization to more complex tasks. In contrast, without CL, the entire solution time can be devoted to the complex tasks rather than being partitioned into easier and difficult tasks. In experiments, this was found to be relevant. Third, the solution of an easier task does not necessarily represent a better initialization to a harder problem in comparison to an alternative random initialization. For example, consider the scenario in Fig. 6. The solution of the simpler task does not serve as a better initialization than a purely random initialization of weights. This is since the final solution requires outreaching steering and possibly reversing of the vehicle. The simpler task just requires forward driving and stopping. This simple example illustrates the need for careful manual selection of suitable easier tasks for CL.

In the course of this work, a plethora of reward shaping methods were tested. These include, first, solving “simpler” tasks by first dismissing obstacles and target angles limited to 30° -deviation from the initial heading. Second, ϵ -tolerances were initially relaxed before gradually decreasing them. Third, it was tested to first solve a task for only the ϵ_d -criterion, then both $(\epsilon_d, \epsilon_\psi)$, and only finally all of $(\epsilon_d, \epsilon_\psi, \epsilon_v)$. Here, also varying sequences (e.g., first ϵ_ψ instead of ϵ_d) were tested. No consistent improvement could be observed for neither of these methods. On the contrary, solving allegedly simpler task reduced available solver time for the original “hard” problems. Without CL the entire solution time can be devoted to the complex tasks. Therefore, the preferred reward design is:

$$r_t = \begin{cases} -\infty, & \text{if } f_t^{\text{crash}} = 1, \\ -1, & \text{otherwise,} \end{cases} \quad (7)$$

in combination with f_t^{goal} from (6), and

$$\Delta p_t = -\sqrt{(x_{t+1} - x_t)^2 + (y_{t+1} - y_t)^2}, \quad (8)$$

$$F_i = \begin{cases} 1, & \text{if } \sum_{\tau=t-T^{\text{goal}}+1}^t f_\tau^{\text{goal}} = T^{\text{goal}}, \\ 0, & \text{otherwise,} \end{cases} \quad (9)$$

where f_t^{crash} is an indicator flag of a vehicle crash. Upon $F_i = 1$, the reinforcement learning problem is considered as solved. For generality, an integral F_i is defined with problems such as the *inverted pendulum* [42] in mind, which require stabilization and are only considered to be solved after stabilization is demonstrated for sufficiently many consecutive T^{goal} time steps. Note, however, that this is not required for an automotive setting. Here, it must be $T^{\text{goal}} = 1$. Only then learning with $v^{\text{goal}} \neq 0$ is possible (see also Section V-D). Other criteria and trade-offs for Δp_t naturally are possible, especially, accumulated curvature of resulting paths, and a minmax objective therefore. The negation is introduced for maximization (“hill climbing” convention). Note that the preferred reward signal is maximal sparse, returning a negative

constant, -1 , for all times up until reaching the target. It represents a *tabula rasa* solution criticized in [39] for its maximal sparsity. Indeed, standalone it was not sufficient to facilitate learning when also accounting for a velocity target v^{goal} . Therefore, *virtual constraints* (VC) on velocity in target proximity are introduced. Thus,

$$v_t^m = \begin{cases} v^m, & \text{if } e_{d,t} \geq R_v^{\text{thresh}}, \\ v^{\text{goal}} + \frac{(v^m - v^{\text{goal}})}{R_v^{\text{thresh}}} e_{d,t}, & \text{otherwise,} \end{cases} \quad (10)$$

is defined, where $m \in \{\text{max}, \text{min}\}$, and R_v^{thresh} is a hyperparameter (e.g., the range-view length or a heuristic constant). Then, the neural network output is scaled as

$$a_t = \begin{bmatrix} \frac{v_t^{\text{max}} - v_t^{\text{min}}}{\delta^{\text{max}} - \delta^{\text{min}}} \\ \frac{v_t^{\text{max}} + v_t^{\text{min}}}{\delta^{\text{max}} + \delta^{\text{min}}} \end{bmatrix} \odot a_t^{\text{NN}} + \begin{bmatrix} \frac{v_t^{\text{max}} - v_t^{\text{min}}}{2} \\ \frac{v_t^{\text{max}} + v_t^{\text{min}}}{2} \end{bmatrix} \quad (11)$$

where \odot here denotes the Hadamard product. Let us legitimize VCs. Since speed is a decision variable it can always be artificially constrained. This justifies the introduction of (10). Here, bounds are set to *affinely* converge towards v^{goal} in the proximity of the goal location. This is a heuristic choice. Note that the affine choice does *not* necessarily imply constant accelerations. This is since (10) is spatially parameterized. Note further that rate-constraints (5) still hold when (11) is applied to the vehicle. For $R_v^{\text{thresh}} = 0$, VCs are dismissed. It was also tested to constrain δ_t . However, this did not accelerate learning. The final heading pose implies circles prohibited from trespassing because of the nonholonomic vehicle. It was also tested to add these as *virtual obstacles*. However, this too did not improve. Finally, note that VCs on velocity artificially introduce hard constraints, parameterized by R_v^{thres} , and thus shape the learning result w.r.t velocity, at least *towards the end* of the trajectory. Two comments are made. First, in receding online operation, with additional frequent resetting of targets, this shaping effect is reduced since only the first control of a planned trajectory is applied. Second, the influence of hyperparameter R_v^{thres} only becomes apparent during parking when following the trajectory up until standstill. However, here no significant velocity changes are desired, such that the R_v^{thres} -choice is not decisive.

To summarize this section. It was illustrated that the design of *rich reward* signals as well as *curriculum learning* can be problematic. Therefore, *maximal sparse rewards* in combination with *virtual constraints* on velocity were proposed.

C. The role of tolerances

Tolerances ϵ hold an important role for two reasons. On one hand, nonzero ϵ -tolerances result in deviations between actually learnt \hat{z}^{goal} and originally desired goal pose z^{goal} . On the other hand, very small ϵ (e.g., $\epsilon_d = 0.1\text{m}$, $\epsilon_\psi = 1^\circ$ and $\epsilon_v = 1\text{km/h}$) prolong learning time. Two scenarios apply.

First, for a network trained on a large-scale and dense grid of training tasks and for small ϵ , during online operation, suitable control commands are naturally interpolated even for setpoints not seen during training. This applies especially when training and online operation are conducted *obstacle-free*. Here, structured task design can be applied optimally, gridding tasks over polar coordinates and velocity. The concept

of interpolation through *encoded motion primitives* within the network is the core advantage over methods relying on look-up tables with stored trajectories, and which require to solve time-critical search problems. For example, in [4] exhaustive search of the entire lattice-graph is conducted online on a GPU. In [8], a total of about 100 motion primitives is considered. Then, online an integer program is solved by enumeration using maximal progress along the centerline as criterion for selection of the best motion primitive. In contrast, for neural feedforward control this search is not required.

Second, the scenario was considered in which existing training hardware does a) not permit large-scale encoding, and b) only permits to use larger ϵ -tolerances to limit training time. Therefore, the following method is devised. First, tuples $(z^{\text{goal}}, z^{\text{goal}})$ are stored for each training task. Then, during online operation, for any setpoint, z^{setpoint} , the closest (according to a criterion) \hat{z}^{goal} from the set of training tasks is searched, before the corresponding z^{goal} is applied to the network controller. Two comments are made. First, in order to reach \hat{z}^{goal} (with zero deviation), z^{goal} must be applied to the network. Therefore, *tuples* need to be stored. Second, even though this method now also includes a search, it still holds an important advantage over lattice-based methods. Namely, through the *compression* of the look-up table in the network weights. Hence, only tuples need to be stored—not entire trajectories. This is especially relevant in view of limited *hardware memory*. Thus, through encoding, potentially many more motion primitives can be stored in comparison to lattice-based methods.

In practice, the first scenario is obviously preferable. It is also implementable for two reasons. First, see Section IV-G for computational opportunities. Second, neural networks have in principle unlimited function approximation capability [43]. Hence, the implementation of the first approach is purely a question of intelligent task setup, and computational power.

D. Main Algorithm – TSHC

Algorithm 1 is proposed for simple gradient-free model-based reinforcement learning. The name is derived from the fact of a) learning from separate training tasks, and b) a hill climbing update of parameters (greedy local search).

Let us elaborate on definitions. Analysis is provided in Section V-E. First, all network parameters are lumped into variable θ . Second, the perturbation step 8 in Algorithm 1 has to be interpreted accordingly. It implies parameter-wise affine perturbations with zero-mean Gaussian noise and spherical variance σ_{pert}^2 . Third, $\mathcal{X}(\cdot)$, $\mathcal{R}(\cdot)$ and $\mathcal{Z}(\cdot)$ in Steps 14-16 denote functional mappings between properties defined in the preceding sections. Fourth, hyperparameters are stated in Step 2. While N_{restarts} , $N_{\text{iter}}^{\text{max}}$, n , N_{tasks} and T^{max} denote lengths of different iterations, $\beta > 1$ is used for updating of σ_{pert} in Step 35 and 37. Fifth, for every restart iteration, i_{restart} , multiple parameter iterations are conducted, at most $N_{\text{iter}}^{\text{max}}$ many. Sixth, in Steps 25 and 29 hill climbing is conducted, when a) all tasks have been solved for current i_{iter} , or b) not all tasks have yet been solved, respectively. Seventh, there are two steps in which an early termination of iteration may occur: Step 21 and 41. The former is a must. Only then learning

Algorithm 1: Task Separation with Hill Climbing (TSHC)

```

1 Input: system model, network structure, training tasks,
   and  $N_{\text{restarts}}$ ,  $N_{\text{iter}}^{\text{max}}$ ,  $n$ ,  $N_{\text{tasks}}$ ,  $T^{\text{max}}$ ,  $\beta$ ,  $\epsilon$ ,  $\sigma_{\text{pert}}^{\text{min}}$ ,  $\sigma_{\text{pert}}^{\text{max}}$ .
2 Initialize  $\theta^* \leftarrow \emptyset$ ,  $N^* \leftarrow 0$ ,  $P^* \leftarrow -\infty$ ,  $J^* \leftarrow 0$ .
3 for  $i_{\text{restart}} = 1, \dots, N_{\text{restarts}}$  do
4   Initialize  $\theta$  randomly, and  $\sigma_{\text{pert}} \leftarrow \sigma_{\text{pert}}^{\text{max}}$ ,  $N_{\text{old}}^{\text{tasks},*} \leftarrow 0$ .
5   for  $i_{\text{iter}} = 1, \dots, N_{\text{iter}}^{\text{max}}$  do
6     % RUN ASYNCHRONOUSLY:
7     for  $i = 1, \dots, n$  do
8       Perturb  $\theta_i \leftarrow \theta + \sigma_{\text{pert}} \zeta$ , with  $\zeta \sim \mathcal{N}(0, I)$ .
9       Initialize  $N_i^{\text{tasks},*} \leftarrow 0$ ,  $P_i \leftarrow 0$ ,  $J_i \leftarrow 0$ .
10      for  $i_{\text{task}} = 1, \dots, N_{\text{tasks}}$  do
11        Initialize  $z_0$  (and LSTM and GRU cells).
12        for  $t = 0, \dots, T^{\text{max}} - 1$  do
13          Read  $(s_t, I_t)$  from  $i_{\text{task}}$ -environment.
14           $a_t \leftarrow \mathcal{X}(s_t, I_t, \theta_i)$ .
15           $(r_t, \Delta p_t, f_t^{\text{goal}}) \leftarrow \mathcal{R}(s_t, I_t, a_t)$ .
16           $z_{t+1} \leftarrow \mathcal{Z}(z_t, a_t)$ .
17           $P_i \leftarrow P_i + \Delta p_t$ .
18           $J_i \leftarrow J_i + r_t$ .
19           $F_i$  according to (9).
20          if  $(F_i == 1) \vee (r_t == -\infty)$  then
21            | Break  $t$ -loop.
22          |  $N_i^{\text{tasks},*} \leftarrow N_i^{\text{tasks},*} + F_i$ .
23        % DETERMINE  $i^*$ :
24        if  $\max_i \{N_i^{\text{tasks},*}\}_{i=1}^n == N_{\text{tasks}}$  then
25          |  $i^* = \arg \max_i \{P_i \mid N_i^{\text{tasks},*} == N_{\text{tasks}}\}_{i=1}^n$ .
26          | if  $P_{i^*} > P^*$  then
27            |  $(\theta^*, N^*, P^*, J^*) \leftarrow (\theta_{i^*}, N_{\text{tasks}}, P_{i^*}, J_{i^*})$ .
28        else
29          |  $i^* = \arg \max_i \{J_i\}_{i=1}^n$ .
30          | if  $(J_{i^*} > J^*) \wedge (P^* == -\infty)$  then
31            |  $(\theta^*, N^*, P^*, J^*) \leftarrow (\theta_{i^*}, N_{i^*}^{\text{tasks}}, P_{i^*}, J_{i^*})$ .
32         $N_{\text{old}}^{\text{tasks},*} \leftarrow N_{i^*}^{\text{tasks},*}$ .
33        % UPDATE PARAMETERS:
34        if  $N_{\text{old}}^{\text{tasks},*} > N_{\text{old}}^{\text{tasks},*}$  then
35          |  $\sigma_{\text{pert}} \leftarrow \max(\frac{1}{\beta} \sigma_{\text{pert}}, \sigma_{\text{pert}}^{\text{min}})$ .
36        else if  $N_{\text{old}}^{\text{tasks},*} < N_{\text{old}}^{\text{tasks},*}$  then
37          |  $\sigma_{\text{pert}} \leftarrow \min(\beta \sigma_{\text{pert}}, \sigma_{\text{pert}}^{\text{max}})$ .
38         $\theta \leftarrow \theta_{i^*}$  and  $N_{\text{old}}^{\text{tasks},*} \leftarrow N_{\text{old}}^{\text{tasks},*}$ .
39        % OPTIONAL:
40        if  $N_i^{\text{tasks},*} == N_{\text{tasks}}$  then
41          | Break  $i_{\text{iter}}$ -loop. % no further refinement step.
42 Output:  $(\theta^*, N^*, P^*, J^*)$ .

```

with $v^{\text{goal}} \neq 0$ is possible. The latter termination criterion in Step 41 is optional. If dismissed, a *refinement step* is implied. Thus, eventhough all N_{tasks} tasks have been solved, parameter iterations (up until $N_{\text{iter}}^{\text{max}}$) are continued. Eight, note that a discount hyperparameter γ , common to gradient-based RL methods [44], is not required. This is since it is irrelevant in the maximally sparse reward setting. Finally, options for parallelization are outlined. In principle, nested parallelization is possible with an inner and outer parallelization of Steps 10-22 and 7-22, respectively. The former refers to N_{tasks} solutions for a given parameter vector θ_i , whereas the latter parallelizes n parameter perturbations. For final experiments, Steps 7-22 were implemented asynchronously.

E. Analysis

According to classifications in [45], TSHC is a gradient-free *instance-based* simulation optimization method, generating new candidate solutions based on only the current solution and *random search* in its neighborhood. Because of its hill climbing (greedy) characteristic, it differs from a) *evolutionary* (population-based) methods that construct solution by combining others typically using weighted averaging [46], [29], and b) from *model-based* methods that use *probability distributions* on the space of solution candidates, see [45] for a survey. In its high-level structure, Algorithm 1 can be related to the industrial strength COMPASS algorithm [47]. Within a global stage, they identify several possible regions with locally optimal solutions. Then, they find local optimal solutions for each of the identified regions. In a third stage, they select the best solution among all identified locally optimal solutions. In our setting, these regions are enforced as the separate training tasks and the best solution for all of these is selected.

An important role is held by σ_{pert} . In combination with sufficiently large n , it must be large enough to permit sufficient exploration such that a network parametrization solving all tasks can be found. In contrast, the effect of decreasing σ_{pert} with an increasing number of solved tasks is that, ideally, a speedup in learning progress results from the assignment of more of solution candidates θ_i closer in variance to a promising parametrization θ , see Step 8. For final experiments, $\sigma_{\text{pert}}^{\text{min}}$ was dismissed to not constrain σ_{pert} -adaptation.

Steps 29-31 are discussed. For the case that for a specific i_{iter} -iteration not all tasks have been solved, $i^* = \arg \max_i \{N_i^{\text{tasks},*}\}_{i=1}^n$ has been considered as an alternative criterion for Step 29. Several remarks can be made. First, Step 29 and the alternative are not equal. This is because, in general, different tasks are solved in a different number of time steps. However, the criteria are *approximately* equivalent for sparse rewards (since J_i accumulates constants according to (7)), and especially for large T^{max} . The core advantage of employing Step 29 in TSHC is that it can, if desired, also be used in combination with *rich* rewards to accelerate learnig progress (if a suitable rich reward signal can be generated). In such a scenario, i^* according to Step 29 is updated towards most promising J_{i^*} , then representing the accumulated *rich* reward. Thus, in contrast to (7), a rich reward could be

represented by a weighted sum of squared errors between state $z_t \in \mathbb{R}^{n_z}$ and a reference $z_t^{\text{ref}} \in \mathbb{R}^{n_z}$,

$$r_t = \begin{cases} -\infty, & \text{if } f_t^{\text{crash}} == 1, \\ -\sum_{l=0}^{n_z-1} \alpha_l (z_t(l) - z_t^{\text{ref}}(l))^2, & \text{otherwise,} \end{cases} \quad (12)$$

where α_l are trade-off hyperparameters and scalar elements of vectors are indexed by l in brackets. Another advantage of the design in Algorithm 1 according to Step 29-31 is its *anytime solution* character. Even if not all N_{tasks} are solved, the solution returned for the tasks that *are* solved, typically is of good quality and optimized according to Steps 29-31.

If for all N_{tasks} tasks there exists a feasible solution for a given system model and a sufficiently expressive network structure parameterized by θ , then Algorithm 1 can find such parametrization for sufficiently large hyperparameters N_{restarts} , $N_{\text{iter}}^{\text{max}}$, n , T^{max} and $\sigma_{\text{pert}}^{\text{max}}$. The solution parametrization θ^* is the result from the initialization Step 4 and parameter perturbations according to Step 8, both nested within multiple iterations. As noted in [48], for optimization via simulation, a global convergence guarantee provides little practical meaning other than reassuring a solution will be found *eventually* when simulation effort goes to infinity. The same reference states that a convergence property is most meaningful if it can help in designing suitable stopping criteria. Here, there are two conceptual levels of stopping criteria: first, the solution of all training tasks, and second, the refinement of solutions.

Control design is implemented hierarchically in two steps. First, suitable *training tasks* (desired motion primitives) are defined. Then, these are *encoded* in the network by the application of TSHC. This has practical implications. First, it encourages to train on *deterministic* tasks. Furthermore, at every i_{iter} , it is *simultaneously* trained on all of these separate tasks. This has the benefit that the best parametrization, θ^* , is clearly defined in Step 25, maximizing the accumulated P -measure over all tasks. Second, it enables to provide *certificates* on the learnt performance. The certificates are given by provision of a) the employed vehicle model, and b) the list of encoded tasks (motion primitives). Note that such certificates cannot be given for the class of *stochastic* continuous action RL algorithms that are derived from the Stochastic Policy Gradient Theorem [49]. This class includes all stochastic actor-critic algorithms, including A3C [50] and PPO [44].

F. Discussion and comparison with related RL work

A discussion of succesful continuous control methods that use neural network for function approximation is given, focusing on one stochastic [44], one deterministic policy gradient method [36], and one evolution strategy [29]. The methods are discussed in relative detail to underline aspects of TSHC.

First, the *stochastic policy gradient* method PPO [44] is discussed. Suppose that a stochastic continus control vector is sampled from a Gaussian distribution parameterized¹ by θ such that $a_t \sim \pi(a_t|s_t, \theta)$. Then,

$$J(\theta) = \mathbb{E}_{s_t, a_t} [g(s_t, a_t \sim \pi(a_t|s_t, \theta))], \quad (13)$$

¹In this setting, mean and variance of the Gaussian distribution are the output of a neural network whose parameters are summarized by lumped θ .

is defined as the expected accumulated and time-discounted reward when at state s_t drawing a_t , and following the stochastic policy for all subsequent times when acting in the simulation environment. Since function $g(s_t, a_t)$ is a priori not known, it is parameterized by $\theta_{V,\text{old}}$ and estimated. Using RL-terminology, in the PPO-setting, $g(s_t, a_t)$ represents the *advantage function*. Then, using the “log-likelihood trick”, and subsequently a first-order Taylor approximation of $\log(\pi(a_t|s_t, \theta))$ around some reference $\pi(a_t|s_t, \theta_{\text{old}})$, the following parameterized cost function is obtained as an *approximation* of (13),

$$\tilde{J}(\theta) = \mathbb{E}_{s_t, a_t} \left[\hat{g}_t(\theta_{V,\text{old}}) \frac{\pi(a_t|s_t, \theta)}{\pi(a_t|s_t, \theta_{\text{old}})} \right]. \quad (14)$$

Finally, (14) is modified to the final PPO-cost function [44]

$$\hat{J}(\theta) = \mathbb{E}_{s_t, a_t} \left[\min \left(\hat{g}_t(\theta_{V,\text{old}}) \frac{\pi(a_t|s_t, \theta)}{\pi(a_t|s_t, \theta_{\text{old}})}, \text{clip} \left(\frac{\pi(a_t|s_t, \theta)}{\pi(a_t|s_t, \theta_{\text{old}})}, 1 - \epsilon, 1 + \epsilon \right) \hat{g}_t(\theta_{V,\text{old}}) \right) \right], \quad (15)$$

whereby the advantage function is estimated by the policy parameterized by $(\theta_{V,\text{old}}, \theta_{\text{old}})$, which is run for T consecutive time steps such that for all t the tuples $(s_t, a_t, r_t, s_{t+1}, \hat{g}_t(\theta_{V,\text{old}}))$ can be added to a *replay buffer*, from which later minibatches are drawn. According to [44], the estimate is $\hat{g}_{T-1}(\theta_{V,\text{old}}) = \kappa_{T-1}$ with $\kappa_{T-1} = r_{T-1} + \gamma V(s_T, \theta_{V,\text{old}}) - V(s_{T-1}, \theta_{V,\text{old}})$, $\hat{g}_{T-2}(\theta_{V,\text{old}}) = \kappa_{T-2} + \gamma \lambda \hat{g}_{T-1}(\theta_{V,\text{old}})$ and so forth until $\hat{g}_0(\theta_{V,\text{old}})$, and where $V(s, \theta_{V,\text{old}})$ represents a *second*, the so-called critic neural network. Then, using uniform randomly drawn minibatches of size M , parameters (θ_V, θ) of both networks are updated according to $\arg \min_{\theta_V} \frac{1}{M} \sum_{i=0}^{M-1} (V(s_i, \theta_V) - (\hat{g}_i(\theta_{V,\text{old}}) - V(s_i, \theta_{V,\text{old}})))^2$ and $\arg \max_{\theta} \frac{1}{M} \sum_{i=0}^{M-1} \mathcal{G}_i(\theta)$, with $\mathcal{G}_i(\theta)$ denoting the argument of the expectation in (15) evaluated at time-index i . This relatively detailed discussion is given to underline following observations. With first the introduction of a parameterized estimator, then a first-order Taylor approximation, and then clipping, (15) is an arguably crude approximation of the original problem (13). Second, the complexity with *two* actor and critic networks is noted. Typically, both are of the same dimensions apart from the output layers. Hence, when not sharing weights between the networks, approximately *twice* as many parameters are required. However, *when* sharing any weights between actor and critic network, then optimization function (15) must be extended accordingly, which introduces another approximation step. Third, note that gradients of both networks must be computed for backpropagation. Fourth, the dependence on *rich* reward signals is stressed. As long as the current policy does not find a solution candidate, in a *sparse* reward setting, all r_i are uniform. Hence, there is no information permitting to find a suitable parameter update direction and all of the computational expensive gradient computations are essentially not usable². Thus, the network parameters are still updated entirely at random. Moreover, *even if* a solution candidate

trajectory was found, it is easily averaged out through the random minibatch update. This underlines the problematic of *sparse* rewards for PPO. Sixth, A3C [50] and PPO [44] are by nature *stochastic* policies, which *draw* their controls from a Gaussian distribution (for which mean and variance are the output of a trained network with current state as its input). Hence, exact repetition of any task (e.g., the navigation between two locations) cannot be guaranteed. It can only be guaranteed if dismissing the variance component and consequently using solely the mean for deterministic control. This can be done in practice, however, represents another approximation step.

Deterministic policy gradient method DDPG [36] is discussed. Suppose a deterministic continuous control vector parameterized such that $a_t = \mu(s_t, \theta)$. Then, the following cost function is defined,

$$J(\theta) = \mathbb{E}_{s_t, a_t} [g(s_t, a_t = \mu(s_t, \theta))] = \mathbb{E}_{s_t} [g(s_t, \mu(s_t, \theta))].$$

Its gradient can now be computed by simply applying the *chain-rule* for derivatives [51]. Introducing a parameterized estimate of $g(s_t, a_t)$, which here represents the *Q-function* or *action value function* (in contrast to the advantage function in above stochastic setting), the final DDPG-cost function [36] is

$$J(\theta) = \mathbb{E}_{s_t} [\hat{g}(s_t, \mu(s_t, \theta), \theta_Q)],$$

Then, using minibatches, critic and actor network parameters (θ_Q, θ) are updated as $\arg \min_{\theta_Q} \frac{1}{M} \sum_{i=0}^{M-1} (\hat{g}(s_i, a_i, \theta_Q) - (r_i + \gamma Q(s_{i+1}, \mu(s_{i+1}, \theta_{\text{old}}), \theta_{Q,\text{old}})))^2$ and $\arg \min_{\theta} \frac{1}{M} \sum_{i=0}^{M-1} Q(s_i, \mu(s_i, \theta), \theta_Q)$, with slowly tracking target network parameters $(\theta_{Q,\text{old}}, \theta_{\text{old}})$. Several remarks can be made. First, the Q-function is updated towards only its *one-step* ahead target. It is obvious that rewards are therefore propagated very slowly. For sparse rewards this is even more problematic than for rich rewards, especially because of the additional danger of averaging out important update directions though random minibatch sampling. Furthermore, and analogous to the stochastic setting, for the sparse reward setting, as long as no solution trajectory was found, all of the gradient computations are not usable and all network parameters are still updated entirely at random. DDPG is an *off-policy* algorithm. In [36], exploration of the simulation environment is achieved according to the current policy plus additive noise following an *Ornstein-Uhlenbeck* process. This is a mean-reverting linear stochastic differential equation [52]. A first-order Euler approximation thereof can be expressed as the action exploration rule $a_t = \mu(s_t, \theta)(1 - P_{\theta}^{\text{OU}}) + P_{\sigma}^{\text{OU}} \epsilon$, $\epsilon \sim \mathcal{N}(0, I)$, with hyperparameters $(P_{\theta}^{\text{OU}}, P_{\sigma}^{\text{OU}}) = (0.15, 0.2)$ in [36]. This detail is provided to stress a key difference between policy gradient methods (both stochastic and deterministic), and methods such as [29] and TSHC. Namely, while the former methods sample controls from the stochastic policy or according to *heuristic* exploration noise before updating parameters using minibatches of *incremental* tuples (s_i, a_i, r_i, s_{i+1}) plus $\hat{g}_i(\theta_{V,\text{old}})$ for PPO, the latter directly work in the *parameter space* via local perturbations, see Step 8 of Algorithm 1. This approach appears particularly suitable when dealing with

²It is mentioned that typically the first, for example, 50000 samples are collected *without* parameter update. However, even then that threshold must be selected, and the fundamental problem still perseveres.

sparse rewards. As outlined above, in such setting, parameter updates according to policy gradient methods are also entirely at random, however, with the computationally significant difference of first an approximately four times as large parameter space and, second, the unnecessary costly solution of non-convex optimization problems as long as no solution trajectory has been found. A well-known issue in training neural networks is the problem of vanishing or exploding gradients. It is particularly relevant for networks with saturating nonlinearities and can be addressed by recent batch [53] and layer normalization [54]. In both normalization approaches, *additional* parameters are introduced to the network which must be learnt (bias and gains). Said issue is not relevant for the proposed gradient-free approach, in which also saturating activation functions are used, see Section V-A.

This paper is originally inspired by and most closely related to [29]. The main differences are discussed. The latter evolutionary (population-based) strategy updates parameters using a *stochastic gradient estimate*. Thus, it updates $\theta \leftarrow \theta + \alpha \frac{1}{n\sigma} \sum_{i=1}^n R_i \zeta_i$, where hyperparameters α and σ denote the learning rate and noise standard deviation, and where R_i here indicates the stochastic scalar return provided by the simulation environment. This weighted averaging approach for the stochastic gradient estimate is not suitable for our control design method when using separate deterministic training tasks in combination with maximally sparse rewards. Here, hill climbing is more appropriate. This is since most of the n trajectory candidates do not end up at z^{goal} and are therefore not useful. Note also that only the introduction of virtual constraints on velocity permitted us to quickly train with maximally sparse rewards. It is well known that for gradient-based training, especially of RNNs, the learning rate (α in [29]) is a critical hyperparameter choice. In the hill climbing setting this issue does not occur. Likewise, *fitness shaping* [46], also used in [29], is not required. Note that above σ has the same role as σ_{pert} . Except, in our setting, it additionally is adaptive according to Steps 29 and 31 in Algorithm 1. As implemented, this is only possible when training on multiple separate tasks. Other differences include the parallelization method in [29], where random seeds shared among workers permit each worker to only need to send and receive the scalar return of an episode to and from each other worker. All perturbations and parameters are then reconstructed locally by each worker (for n workers there are n reconstructions at each parameter-iteration step). This requires precise control of each worker and can in rare cases lead to differing CPU utilizations among workers due to differing episode lengths. Therefore, they use a capping strategy on maximal episode length. Our proposed method is less sophisticated with *one* synchronized parameter update, which is then sent to all workers.

VI. EXPERIMENTS

This section highlights different aspects of Algorithm 1. Interpretations are summarized in Section VI-E. For all experiments, both continuous steering and velocity control are required. Throughout, tolerances are set as $(\epsilon_d, \epsilon_\psi, \epsilon_v) = (1, 10\pi/180, 10/3.6)$, see also Section V-C.

In Section VI-A, for the implementation of the two policy gradient methods, Tensorflow (without GPU-support) was

TABLE I. Experiment 1. Number of scalar parameters (weights) that need to be identified for DDPG, PPO and TSHC, respectively. TSHC requires to identify the least by a large margin. In general, roughly by a factor 4. The fact that PPO here requires *exactly* four times the number of parameters of TSHC is a special case for $n_a = 2$ (not generalizable for arbitrary n_a).

	DDPG	PPO	TSHC
N_{var}	19078	18440	4610

TABLE II. Experiment 2a. Learning 5 tasks. Comparison of six architectures A1-A6. Hyperparameters are selected as $n = 2000$, $T_{\text{max}} = 100$, and terminating upon the first solution found (no refinement step, no additional restart). Results are average over 5 runs. The total number of parameters to be identified, the number of iterations until the first solution solving all tasks, the total accumulated pathlength and solve time for Algorithm 1 are denoted by N_{var} , \bar{N}_{iter}^* , \bar{P}^* and \bar{T}^* , respectively.

	A1	A2	A3	A4	A5	A6
N_{var}	4610	4610	118	166	169	12930
\bar{N}_{iter}^*	19	6	5	5	5	13
\bar{P}^*	152.7	152.6	150.51	148.31	152.4	157.6
\bar{T}^*	481.1	141.3	144.9	165.95	110.6	367.8

used. All experiments were conducted on a laptop running Ubuntu 16.04 equipped with an Intel Core i7 CPU @2.80GHz×8, 15.6GB of memory, and using Python 2.7. For the implementation of Algorithm 1, the only libraries employed are Python’s `numpy` and `multiprocessing`.

A. Experiment 1: Comparison with policy gradient methods

To underline conceptual differences between TSHC and the two policy gradient methods DDPG [36] and PPO [44], a freeform navigation task with $z_0 = [0, 0, 0, 0]$ and $z^{\text{goal}} = [20, 0, \pi/4, 0]$ was considered. The same network architecture from [44] is used: a fully-connected MLP with two hidden layers of 64 units before the output layer. Eventhough this is the basic setup, considerable differences between DDPG, PPO and TSHC are implied. First, both DDPG and PPO are each composed of a total of four networks: one actor, one critic, one actor target and one critic target network. For DDPG, further parameters result from batch normalization [53]. The number of parameters N_{var} that need to be identified are indicated in Table I. To enable a fair comparison, all of DDPG, PPO and TSHC are permitted to train on 1000 full rollouts according to their methods, whereby each rollout lasts at most $T_{\text{max}} = 100$ timesteps. Thus, for TSHC, $N_{\text{restarts}} = 1$ and $n = 1000$ are set. For both PPO and DDPG, this implies 1000 iterations. The results are summarized in Fig. 7 and 8. The following observations can be made. First, in comparison to TSHC, for both DDPG and PPO significantly more parameters need to be identified. Second, DDPG and PPO do *not* solve the task based on 1000 training simulations. In contrast, as Fig. 7 demonstrates, TSHC has a much better exploration strategy resulting from noise perturbations in *parameter space* and also solves the task in just 2.1s. Finally, note that no σ_{pert} -iteration is conducted. It is not applicable since a *single* task is solved with an initial $\sigma_{\text{pert}}^{\text{max}} = 10$. Because of these findings (other target poses were also tested with qualitatively equivalent results) and the discussion in Section V-F, specifically about the handling of *sparse rewards* and the fact that DDPG and PPO have no useful gradient direction for their parameter update or may average these out through random minibatch

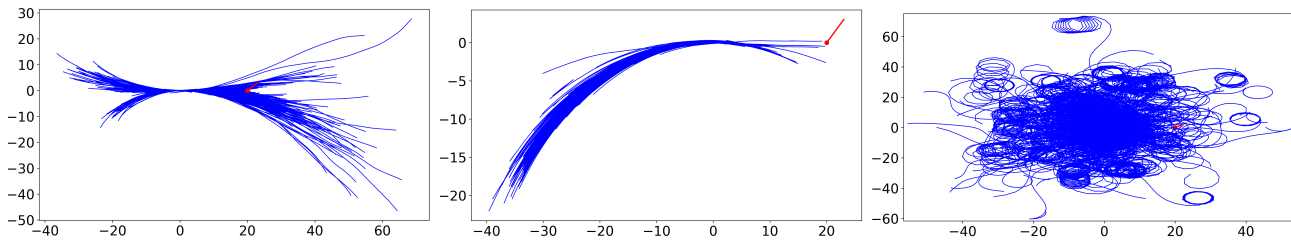


Fig. 7. Experiment 1. 1000 training trajectories resulting from the application DDPG (Left), PPO (Middle) and TSHC (Right), respectively. The effect of virtual constraints on velocity is particularly visible for DDPG. For the given hyperparameter setting ([44, Table 3] and $T_{\max} = 100$), the trajectories for PPO have little spread and are favoring reverse driving. TSHC has a much better exploration strategy resulting from noise perturbations in the parameter space. The task is solved by TSHC according to Fig. 8.

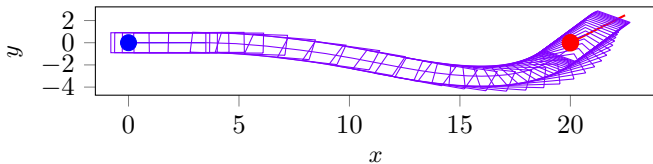


Fig. 8. Experiment 1. The network controller trained by the TSHC method solves the task in only 2.1 seconds, when terminating upon the first solution found (no refinement step, no additional restart). Rectangular vehicle dimensions are displayed. Blue and red ball and indicators visualize z_0 and z^{goal} .

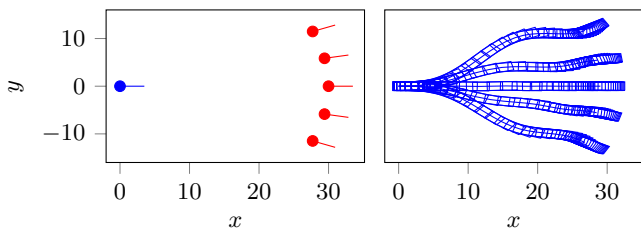


Fig. 9. Experiment 2a. Learning 5 tasks. (Left) Problem formulation with start (blue) and end (red) positions as well as headings. Start and desired end velocities are zero. (Right) LSTM-solution after less than 150s training time. Vehicle dimensions are displayed.

sampling, the focus in the subsequent sections is on TSHC and its analysis.

B. Experiment 2: Zone navigation without obstacles

Various zone navigation experiments without obstacles are conducted. Therefore, to eliminate the influence of the I-network park, NETW_{sI} and $\text{NETW}_{\bar{s}}$ here coincide.

For Experiment 2a, six different architectures (A1-A6) are compared. Results are summarized in Table II and Fig. 9. For A1 and A2, the same architecture from [44] is considered: a fully-connected MLP with two hidden layers of 64 units before the output layer. A1 and A2 solely differ by the absence and inclusion of *adaptive* σ_{pert} according to Algorithm 1. For A3 and A4, a single GRU- and LSTM-cell before the output layer are considered, respectively. For A5, a fully-connected MLP with two hidden layers of 10 and 9 units before the output layer is used, such that approximately the same number of parameters as for A4 are identified. For A6, a MLP with four hidden layers of 64 units before the output layer is considered. Several observations can be made. First, as the comparison of A1-A2 solve times shows, adaptive σ_{pert} is useful in providing speedup. Due to adaptive σ_{pert} , the A6-network which is almost 3-times larger than A1, can encode the five tasks 23.6% faster

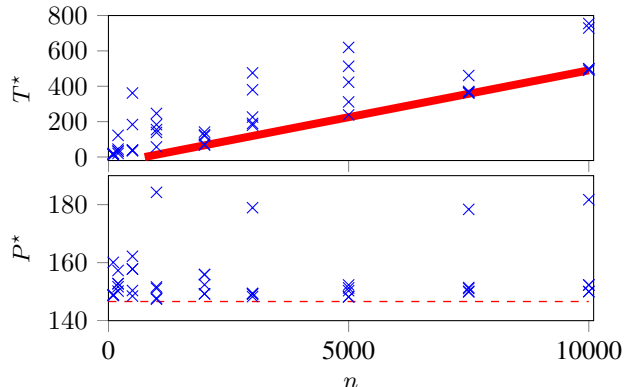


Fig. 10. Experiment 2b. The results for A2 as a function of different n are displayed. The problem setup is as in Fig. 9. For each n , five restarts are conducted. For each restart, the i_{iter} -loop is terminated upon the first solution found (no refinement step). The solid red line indicates the interpolated lower bound on solve times. The fine red dashed line denotes the minimum accumulated pathlength (146.6m) after $N_{\text{iter}} = 100$ with refinement step.

than A1, which does not adapt σ_{pert} . Second, single GRU- and LSTM-cells as well as a smaller MLP (A5) with few parameters can encode the tasks, too.

For Experiment 2b, the effect of n is analyzed for A2, see Fig. 10. As expected, solve times clearly increase with increasing n . However, solution quality (measured by total accumulated pathlength) is not affected in the same manner. Suboptimal solutions typically include an unnecessary pathlength-prolonging circular turn before reaching a goal position. Importantly, large n do not automatically imply best results. Often a large spread in T^* and P^* over different restarts could be observed. This underlines the importance of multiple restarts and refinement steps for optimized solutions.

For Experiment 2c, A4 (a single LSTM-cell before the output layer) is used for the learning of 4 tasks with goal positions distributed symmetrically on a circle, see Fig. 11.

For Experiment 2d, see Fig. 12. The importance of conducting multiple restarts is underlined. Not always all tasks could be solved for every restart.

C. Experiment 3: Navigation with an obstacle

The following problem is addressed: overtaking of an obstacle if it exists, and straight road following if there is none. Therefore, two tasks are formulated: one with and one without any obstacle. A relative velocity difference between an ego and a lead car of 30km/h is assumed, and $z_0 = [0, 0, 0, 30/3.6]$ and

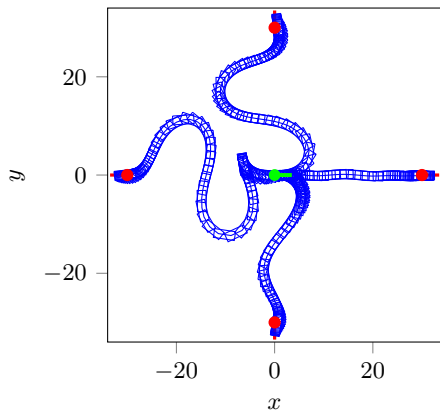


Fig. 11. Experiment 2c. Learning 4 tasks. Start (green) and end (red) positions as well as headings are displayed, distributed symmetrically along a circle of radius 30m. Start and desired end velocities are zero. The LSTM-solution (A4-architecture with $N_{\text{var}} = 166$) after 435.8s training time and $N_{\text{iter}}^* = 16$ is visualized. Note that one task (with $x^{\text{goal}} = -30$) is solved by driving *reverse* for some part. This is enabled by system modeling according to Section IV-E. Since not conducting any restarts and refinement steps, overall suboptimal (non-minimum accumulated pathlength) trajectories result.

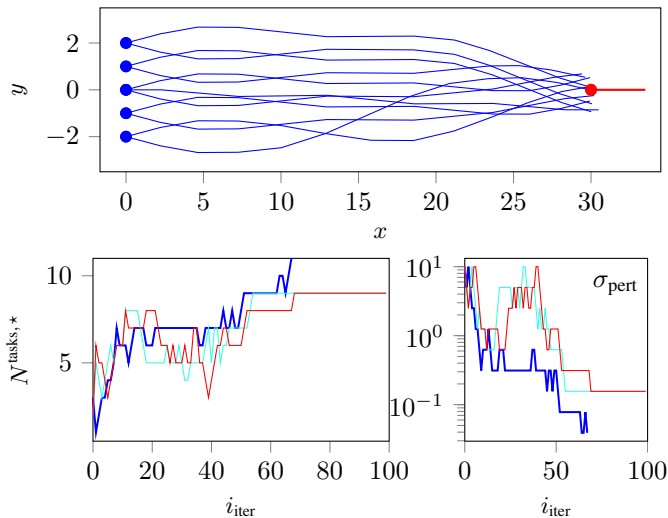
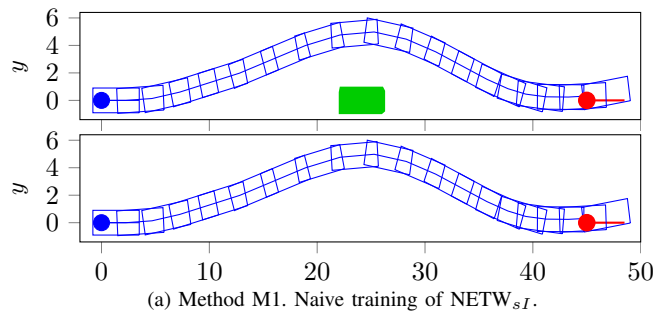


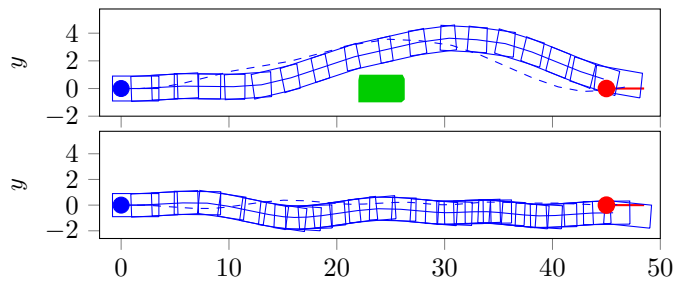
Fig. 12. Experiment 2d. Learning 11 tasks. Architecture A2 is employed. One out of three restarts solved all tasks within $N_{\text{iter}}^{\text{max}} = 100$ for each restart and $n = 100$. No refinement steps are conducted, which explains the asymmetry of trajectories. The total training time was 620.1s.

$z^{\text{goal}} = [45, 0, 0, 30/3.6]$ are set. A front range-view of 20m is selected such that late obstacle detection is simulated. A rear range-view of 10m is assumed. The obstacle is located at $x = 22$. Thus, it is initially not seen. Pixel resolution is set to 0.5m/pixel: 60 and 20 pixels over the entire range view length of 30m and width of 10m, respectively. See also Fig. 3.

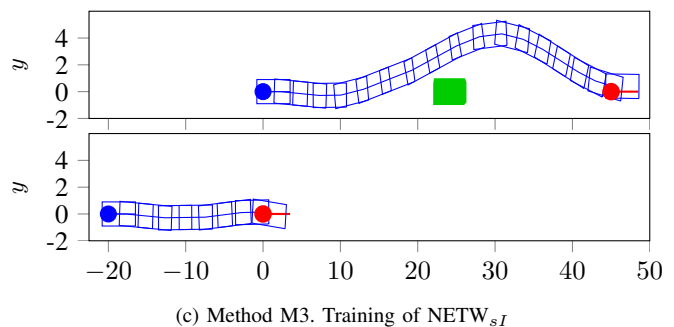
First, NETW_{sI} according Fig. 4 is trained, setting FC-layers with 64 units for each of S-, I- and C-part, and additionally $\Gamma = 1$. Thus, input dimensions are $n_s(1 + \Gamma) = 8$ and $n_I(1 + \Gamma) = 80$, and $N_{\text{var}} = 14146$. A typical learning result is displayed in Fig. 13(a). This result was not expected. While the minimum accumulated pathlength criterion theoretically guarantees a global optimum (by nonnegativity of pathlength and a single obstacle guaranteeing trajectory feasibility), it turned out to be very difficult to escape local optima. The



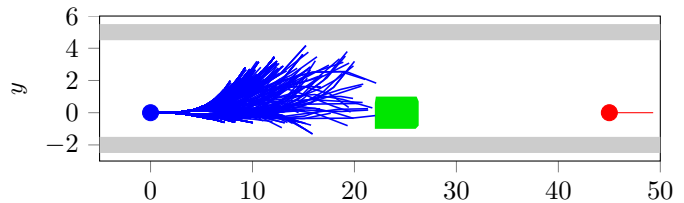
(a) Method M1. Naive training of NETW_{sI} .



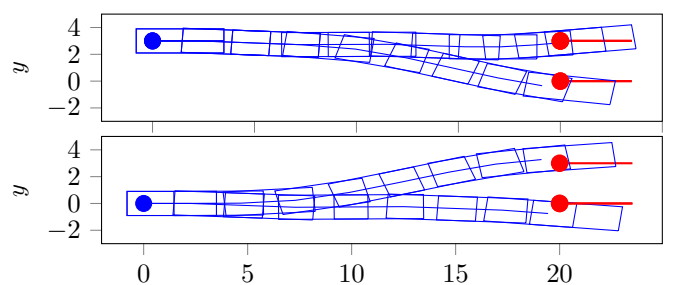
(b) Method M2. Hierarchical training with *rich* rewards in the second stage. Dashed lines indicate references obtained in the first stage.



(c) Method M3. Training of NETW_{sI}



(d) Method M4. Introduction of road bounds (gray). Display of a training step with $n = 1000$ exploration trajectories (without vehicle dimensions). Upon any crash with either a road bound or the obstacle, the time-rollout is interrupted.



(e) Method M5. Learning 4 tasks according to $\text{NETW}_{\bar{s}}$. Only for clarity, the trajectories are partitioned into two plots. The LSTM-architecture A4 ($N_{\text{var}} = 166$) is employed. After 215.3s training time and $N_{\text{iter}}^* = 7$, the four tasks are learnt (no additional restart or refinement step).

Fig. 13. Experiment 3. For better illustration, obstacle avoidance and road following task are separated into two subplots.

trajectory solving the more complex OA-task automatically also solves the simpler task without obstacle. Qualitatively identical behavior was observed when replacing FC-layers by LSTM-cells. Note that when replacing both S- and I-part by LSTM-cells, 58154 parameters need to be identified.

Therefore, an alternative two-step method was tested:

- 1) Solve each task *isolatedly* by Algorithm 1 (with sparse rewards), and store the resulting trajectories as $z_t^{\text{ref},j_{\text{task}}}$, $\forall t = 0, \dots, T^{j_{\text{task}}}$, $\forall j_{\text{task}} = 1, \dots, N_{\text{tasks}}$.
- 2) Solve another RL-problem by Algorithm 1, now simultaneously treating *all* tasks and using *rich* rewards according to (12), with $z_t^{\text{ref},j_{\text{task}}}$ from Step 1 serving as references to obtain $r_t^{j_{\text{task}}}$, $\forall t = 0, \dots, T^{j_{\text{task}}}$, $\forall j_{\text{task}} = 1, \dots, N_{\text{tasks}}$.

Variants are a) to also include controls as references in the rich reward signal, and b) to not terminate the t -iteration upon exceeding $T^{j_{\text{task}}}$, but instead maintaining $z_{T^{j_{\text{task}}}}^{\text{ref},j_{\text{task}}}(l)$ as reference, $\forall t > T^{j_{\text{task}}}$. This two-step method appears appealing because it permits to first optimize each task isolatedly to a desired performance. However, it has two caveats. First, it requires to solve $(N_{\text{tasks}} + 1)$ RL-problems, which is time-consuming. Second, the time-reference tracking over different tasks is difficult. As Fig. 13(b) illustrates, both tasks are learnt, however, the second task trajectory (when not encountering any obstacle) exhibits suboptimal wiggles. The third and most important caveat is that it requires to set hyperparameters α_l , $\forall l$, to trade-off different *units* (meters, radians, and m/s) within the state vector. These were found to be very influential. For the result in Fig. 13(b), $\alpha_l = 1$ for $l = 0, 1$ and $\alpha_l = 0$ for $l = 2, 3$ are set, thereby only considering x, y -coordinates, both measured in meters. This setting, however, turned out to not be sufficient to solve tasks with major steering actuation such as Experiment 2c. Conducting various experiments with above method further consolidated our preference for sparse reward signals. This is since for maximally sparse rewards, different units within the state vector are irrelevant.

For a third method, the original tasks are reformulated by recalibrating (z_0, z^{goal}) -combinations for the case with and without obstacle, see Fig. 13(c). For the second task, $x_0 = -20$ and $z^{\text{goal}} = 0$ are set in regard of the front range-view of 20m. After the (z_0, z^{goal}) -resetting, the same training technique from M1 was applied (with $N_{\text{var}} = 14146$). Now, both tasks are learned, and the original problem formulated at the beginning of this section is solved by resetting (z_0, z^{goal}) -combinations upon first obstacle detection.

Fourth, the influence of road bounds on learning progress was analyzed. In addition, any exploration trajectory is dismissed as soon $v_t < 0$ or $x_t < 0$. Fig. 13(d) visualizes the effect for $n = 1000$ after $i_{\text{iter}} = 5$. Note that because of different velocities, the pixel-discretization resolution, and discretization of obstacle edges crashes are detected irregularly. Because of the many crashes and consequent discarding as potential candidates for the next training iteration, it may (and frequently did) happen that *none* of the n candidates can be used for a parameter update for current i_{iter} . Hence, learning progress is significantly hindered.

Fifth, motivated by the last observations, NETW_{s} was revised for the problem. In fact, the problem can be solved by a) sequentially conducting a lane change, overtaking the

obstacle in parallel, before conducting a second lane change if there exists an obstacle, and b) just maintaining the current lane in case there is no obstacle. Therefore, 4 training tasks can be defined. The front range view horizon of 20m is used as reference for the lane change, implying a lane-change upon the first possible obstacle detection. Fig. 13(e) illustrates the learning results. Note that in general only 3 task formulations, or even only two when permitting control mirroring, can be sufficient for problem solution.

D. Inverted Pendulum

The discussion of tolerance levels in Section V-C motivated to consider an alternative method for tasks requiring stabilization. An analogy to optimal control is drawn. In linear finite horizon MPC, closed-loop stability can be guaranteed through a *terminal state constraint set* which is invariant for a *terminal controller*, often a linear quadratic regulator (LQR), see [55]. In a RL setting, the following procedure was considered. First, design a LQR for stabilization. Second, compute the *region of attraction* of the LQR controller [56, Sect. 3.1.1]. Third, this region of attraction can now be used as stopping criterion, *replacing* the heuristic ϵ -tolerance selection.

For evaluation, the inverted pendulum system equations and parameters from [42] were adopted (four states, one input). However, in contrast to [42], which assumes just two discrete actions (maximum and minimum actuation force), here a *continuous* control variable is assumed which is limited by the two bounds, respectively. There are two basic problems: stabilization in the upright position with initial state in the same position, as well as a swing-up from the hanging position plus consequent stabilization in the upright position. For the application of TSHC, $(N_{\text{restarts}}, N_{\text{iter}}^{\text{max}}, n, T^{\text{max}}, \beta, \sigma_{\text{pert}}^{\text{max}}) = (3, 100, 100, 500, 2, 10)$ are set, and the A2-architecture is used. The following remarks can be made. First, the swing-up plus stabilization task was solved in $T^* = 43.5\text{s}$ runtime of TSHC (without refinement step) and using sparse rewards (only obtained in the upright position $\pm 12^\circ$). For all three restarts a valid solution was generated. Note that $T^{\text{max}} = 500$ in combination with a sampling time [42] of 0.02s corresponds to 10s simulation time. Stabilization in the upright position was achieved from 2.9s on. Rich reward signals were also tested, exploiting the deviation from current to goal angle as measure. However, they did not accelerate learning.

In another experiment, the objective was to *simultaneously* encode the following *two* tasks in the network: stabilization in the upright position with initial state in the same position, and a swing-up from the hanging position plus consequent stabilization in the upright position. The runtime of TSHC (without refinement step) was $T^* = 264.4\text{s}$, with 2 of 3 restarts returning a valid solution and using sparse rewards. Instead of learning both tasks simultaneously according to TSHC, it was also attempted to learn them by selecting one of the two tasks at random at every i_{iter} , and consequently conducting Step 6-41. Since the two tasks are quite different, this procedure could not encode a solution for *both* tasks. This is mentioned to exemplify the importance of training *simultaneously* on separate tasks, rather than training on a single tasks with (z_0, z^{goal}) combinations varying over i_{iter} .

Finally, for system parameters [42], it was observed that the continuous control signal was mostly operating at saturated actuation bounds (switching in-between). This is mentioned for two reasons. First, aforementioned LQR-strategy could therefore never be applied since LQR assumes absence of state and input constraints. Second, it exemplifies the ease of RL-workflow. A combination of network parametrization, TSHC, and a discretization scheme (Euler or Runge-Kutta) enables quick nonlinear control design, even without system insights.

E. Discussion of experiments and summary of findings

First, for automotive applications our preferred network architecture clearly is $\text{NETW}_{\bar{s}}$. Training the alternative NETW_{sI} has several disadvantages: a much larger network sizes due to the I-part, slow learning progress in constrained environments and the difficulty in shaping desired learning results. In contrast, $\text{NETW}_{\bar{s}}$ permits fast learning due to perturbations in the parameter space in combination with obstacle-free freeform navigation tasks, which for sufficiently large T^{\max} naturally guarantee feasibility of solution trajectories. Then, for obstacle avoidance, receding horizon setpoint setting becomes crucial, using I_t as a filter to reset z^{goal} , for example, upon predicted obstacle crash to account for vehicle dimensions or for adaptation of v^{goal} based on, e.g., detected road surface.

Second, the employment of *sparse rewards* for training in combination with *virtual constraints* in setpoint-proximity has several advantages. It naturally avoids the need to introduce trade-off hyperparameters for the weighting of states in different units. And, it permits a solution trajectory between z_0 and z^{goal} to naturally evolve without biasing it by provision of a rich reference to track.

Third, several guidelines for the four key hyperparameters (n , β , N_{restarts} , N_{iter}^{\max}) were identified. Foremost, the importance of multiple restarts is highlighted. Second, n is the most influential hyperparameter. It was found that huge n do not automatically translate to optimal solutions, but always significantly prolong learning duration. For both learning time and solution quality, it is recommended to start with small n in combination with a higher N_{iter}^{\max} to enable multiple iterations over parameters, and to only incrementally increase n when not all tasks could be solved. By $\beta > 1$ it can be controlled how much σ_{pert} is adapted between two parameter iterations (the smaller the more conservative). Testing $\beta = 2$ and $\beta = 1.3$, it was found that the more aggressive $\beta = 2$ always outperformed. In general, adaptive σ_{pert} was found to clearly improve learning speed. Note that our logic for σ_{pert} adaptation differs from [46, Alg. 5 and 6], where also adaptive σ_{pert} is used, however, based on a stochastic gradient estimate.

Fourth, the discussion on ϵ -levels is also related to the decision on system modeling in either the absolute or a road-aligned coordinate system. In contrast to the *spatial-based* convex optimization method from Section II, for two reasons the absolute coordinate framework is clearly favored. First, in contrast to an online-solving approach, spatial parameterization is now not needed for the avoidance of reference velocity-related issues [11]. This is since training tasks are encoded *offline*. Second, the road-aligned coordinate framework is always created online during road-following. It is thus much

more difficult to train offline for varying road shapes, rather than to train on setpoints in an absolute coordinate frame.

VII. CONCLUSION

In the context of automated vehicles, a method for the design of model-based feedforward controllers parameterized by deep neural networks was presented. For this method, a suitable closed-loop architecture was identified, and a simple gradient-free reinforcement learning algorithm labeled TSHC was developed for the identification of network parameters. The concept of a) training on separate tasks with the purpose of encoding motion primitives within the network, and b) employing sparse rewards in combinations with virtual actuator constraints on velocity in setpoint proximity were specifically advocated. The presented method is not limited to automated driving. Most real-world learning applications for control systems, especially in robotics, are characterized by a) sparse rewards, and b) the availability of high-fidelity system models that can be leveraged for offline training.

Subject of ongoing work is the implementation of large-scale experiments based on a high-fidelity vehicle model. Therefore, the method for a) task design and b) the logic for the selection of setpoints, after a filtering step through I_t , must first be formalized. In the presented form, time-scheduling along spatial waypoints [11] is not enabled. Therefore, z_t and z^{goal} may be extended by t and t^{goal} , respectively.

REFERENCES

- [1] B. Paden, M. Čáp, S. Z. Yong, D. Yershov, and E. Frazzoli, "A survey of motion planning and control techniques for self-driving urban vehicles," *IEEE Transactions on Intelligent Vehicles*, vol. 1, no. 1, pp. 33–55, 2016.
- [2] S. Karaman, M. R. Walter, A. Perez, E. Frazzoli, and S. Teller, "Anytime motion planning using the RRT," in *IEEE Conference on Robotics and Automation*, pp. 1478–1483, 2011.
- [3] D. Dolgov, S. Thrun, M. Montemerlo, and J. Diebel, "Path planning for autonomous vehicles in unknown semi-structured environments," *The International Journal of Robotics Research*, vol. 29, no. 5, pp. 485–501, 2010.
- [4] M. McNaughton, C. Urmson, J. M. Dolan, and J.-W. Lee, "Motion planning for autonomous driving with a conformal spatiotemporal lattice," in *IEEE Conference on Robotics and Automation*, pp. 4889–4895, 2011.
- [5] E. Frazzoli, M. A. Dahleh, and E. Feron, "A hybrid control architecture for aggressive maneuvering of autonomous helicopters," in *IEEE Conference on Decision and Control*, vol. 3, pp. 2471–2476, 1999.
- [6] T. Schouwenaars, B. Mettler, E. Feron, and J. P. How, "Robust motion planning using a maneuver automation with built-in uncertainties," in *IEEE American Control Conference*, vol. 3, pp. 2211–2216, 2003.
- [7] A. Gray, Y. Gao, T. Lin, J. K. Hedrick, H. E. Tseng, and F. Borrelli, "Predictive control for agile semi-autonomous ground vehicles using motion primitives," in *IEEE American Control Conference*, pp. 4239–4244, 2012.
- [8] A. Liniger, A. Domahidi, and M. Morari, "Optimization-based autonomous racing of 1:43 scale rc cars," *Optimal Control Applications and Methods*, vol. 36, no. 5, pp. 628–647, 2015.
- [9] P. Falcone, F. Borrelli, J. Asgari, H. E. Tseng, and D. Hrovat, "Predictive active steering control for autonomous vehicle systems," *IEEE Transactions on Control Systems Technology*, vol. 15, no. 3, pp. 566–580, 2007.
- [10] M. Graf Plessen, D. Bernardini, H. Esen, and A. Bemporad, "Spatial-based predictive control and geometric corridor planning for adaptive cruise control coupled with obstacle avoidance," *IEEE Transactions on Control Systems Technology*, 2017.
- [11] M. Graf Plessen, "Trajectory planning of automated vehicles in tube-like road segments," in *IEEE Conference on Intelligent Transportation Systems*, pp. 83–88, 2017.
- [12] M. Graf Plessen, P. F. Lima, J. Mårtensson, A. Bemporad, and B. Wahlberg, "Trajectory planning under vehicle dimension constraints using sequential linear programming," in *IEEE Conference on Intelligent Transportation Systems*, pp. 108–113, 2017.

- [13] D. A. Pomerleau, "Alvin: An autonomous land vehicle in a neural network," in *Advances in Neural Information Processing Systems*, pp. 305–313, 1989.
- [14] M. Bojarski, D. Del Testa, D. Dworakowski, B. Firner, B. Flepp, P. Goyal, *et al.*, "End to end learning for self-driving cars," *arXiv preprint arXiv:1604.07316*, 2016.
- [15] S. Chen, S. Zhang, J. Shang, B. Chen, and N. Zheng, "Brain inspired cognitive model with attention for self-driving cars," *arXiv preprint arXiv:1702.05596*, 2017.
- [16] C. Chen, A. Seff, A. Kornhauser, and J. Xiao, "Deepdriving: Learning affordance for direct perception in autonomous driving," in *IEEE International Conference on Computer Vision*, pp. 2722–2730, 2015.
- [17] H. Xu, Y. Gao, F. Yu, and T. Darrell, "End-to-end learning of driving models from large-scale video datasets," *arXiv preprint arXiv:1612.01079*, 2016.
- [18] C. Paxton, V. Raman, G. D. Hager, and M. Kobilarov, "Combining neural networks and tree search for task and motion planning in challenging environments," *arXiv preprint arXiv:1703.07887*, 2017.
- [19] C. Urmson, J. Anhalt, D. Bagnell, C. Baker, R. Bittner, M. Clark, J. Dolan, D. Duggins, T. Galatali, C. Geyer, *et al.*, "Autonomous driving in urban environments: Boss and the urban challenge," *Journal of Field Robotics*, vol. 25, no. 8, pp. 425–466, 2008.
- [20] T. D. Gillespie, "Vehicle dynamics," *Warren dale*, 1997.
- [21] R. Rajamani, *Vehicle dynamics and control*. Springer Science & Business Media, 2011.
- [22] T. Glasmachers, "Limits of end-to-end learning," *arXiv preprint arXiv:1704.08305*, 2017.
- [23] National Highway Traffic Safety Administration, "Traffic safety facts, 2014: a compilation of motor vehicle crash data from the fatality analysis reporting system and the general estimates system. dot hs 812261," *Department of Transportation, Washington, DC*, 2014.
- [24] D. Kuchin, P. Lega, A. Orlov, V. Koledov, and A. Irzhak, "The smallest and the fastest shape memory alloy actuator for micro-and nanorobotics," in *IEEE Conference on Manipulation, Automation and Robotics at Small Scales*, pp. 1–4, 2017.
- [25] M. Graf Plessen, D. Bernardini, H. Esen, and A. Bemporad, "Multi-automated vehicle coordination using decoupled prioritized path planning for multi-lane one-and bi-directional traffic flow control," in *IEEE Conference on Decision and Control*, pp. 1582–1588, 2016.
- [26] J. Long, E. Shelhamer, and T. Darrell, "Fully convolutional networks for semantic segmentation," in *IEEE Conference on Computer Vision and Pattern Recognition*, pp. 3431–3440, 2015.
- [27] A. Bemporad, M. Morari, V. Dua, and E. N. Pistikopoulos, "The explicit linear quadratic regulator for constrained systems," *Automatica*, vol. 38, no. 1, pp. 3–20, 2002.
- [28] Y. Wang and S. Boyd, "Fast model predictive control using online optimization," *IEEE Transactions on Control Systems Technology*, vol. 18, no. 2, pp. 267–278, 2010.
- [29] T. Salimans, J. Ho, X. Chen, and I. Sutskever, "Evolution strategies as a scalable alternative to reinforcement learning," *arXiv preprint arXiv:1703.03864*, 2017.
- [30] T. Akiba, S. Suzuki, and K. Fukuda, "Extremely large minibatch sgd: Training resnet-50 on imagenet in 15 minutes," *arXiv preprint arXiv:1711.04325*, 2017.
- [31] Nvidia, "Tesla P100." <https://images.nvidia.com/content/tesla/pdf/nvidia-tesla-p100-PCIe-datasheet.pdf>, 2016.
- [32] F. A. Gers, N. N. Schraudolph, and J. Schmidhuber, "Learning precise timing with lstm recurrent networks," *Journal of Machine Learning Research*, vol. 3, no. Aug, pp. 115–143, 2002.
- [33] A. Graves and N. Jaitly, "Towards end-to-end speech recognition with recurrent neural networks," in *International Conference on Machine Learning*, pp. 1764–1772, 2014.
- [34] K. Cho, B. Van Merriënboer, C. Gulcehre, D. Bahdanau, F. Bougares, H. Schwenk, and Y. Bengio, "Learning phrase representations using rnn encoder-decoder for statistical machine translation," *arXiv preprint arXiv:1406.1078*, 2014.
- [35] R. Jozefowicz, W. Zaremba, and I. Sutskever, "An empirical exploration of recurrent network architectures," in *International Conference on Machine Learning*, pp. 2342–2350, 2015.
- [36] T. P. Lillicrap, J. J. Hunt, A. Pritzel, N. Heess, T. Erez, Y. Tassa, D. Silver, and D. Wierstra, "Continuous control with deep reinforcement learning," *arXiv preprint arXiv:1509.02971*, 2015.
- [37] R. S. Sutton and A. G. Barto, *Reinforcement learning: An introduction*, vol. 1. MIT press Cambridge, 1998.
- [38] Y. Bengio, J. Louradour, R. Collobert, and J. Weston, "Curriculum learning," in *International Conference on Machine Learning*, pp. 41–48, ACM, 2009.
- [39] J. Randlov and P. Alstrom, "Learning to drive a bicycle using reinforcement learning and shaping," in *International Conference on Machine Learning*, pp. 463–471, 1998.
- [40] J. Koutník, J. Schmidhuber, and F. Gomez, "Online evolution of deep convolutional network for vision-based reinforcement learning," in *International Conference on Simulation of Adaptive Behavior*, pp. 260–269, Springer, 2014.
- [41] N. Heess, S. Sriram, J. Lemmon, J. Merel, G. Wayne, Y. Tassa, *et al.*, "Emergence of locomotion behaviours in rich environments," *arXiv preprint arXiv:1707.02286*, 2017.
- [42] C. W. Anderson, "Learning to control an inverted pendulum using neural networks," *IEEE Control Systems Magazine*, vol. 9, no. 3, pp. 31–37, 1989.
- [43] H. T. Siegelmann and E. D. Sontag, "Turing computability with neural nets," *Applied Mathematics Letters*, vol. 4, no. 6, pp. 77–80, 1991.
- [44] J. Schulman, F. Wolski, P. Dhariwal, A. Radford, and O. Klimov, "Proximal policy optimization algorithms," *arXiv preprint arXiv:1707.06347*, 2017.
- [45] M. C. Fu, F. W. Glover, and J. April, "Simulation optimization: a review, new developments, and applications," in *IEEE Winter Simulation Conference*, pp. 13–pp, IEEE, 2005.
- [46] D. Wierstra, T. Schaul, T. Glasmachers, Y. Sun, J. Peters, and J. Schmidhuber, "Natural evolution strategies," *Journal of Machine Learning Research*, vol. 15, no. 1, pp. 949–980, 2014.
- [47] J. Xu, B. L. Nelson, and J. Hong, "Industrial strength compass: A comprehensive algorithm and software for optimization via simulation," *ACM Transactions on Modeling and Computer Simulation*, vol. 20, no. 1, p. 3, 2010.
- [48] L. J. Hong and B. L. Nelson, "A brief introduction to optimization via simulation," in *IEEE Winter Simulation Conference*, pp. 75–85, 2009.
- [49] R. S. Sutton, D. A. McAllester, S. P. Singh, and Y. Mansour, "Policy gradient methods for reinforcement learning with function approximation," in *Advances in Neural Information Processing Systems*, pp. 1057–1063, 2000.
- [50] V. Mnih, A. P. Badia, M. Mirza, A. Graves, T. Lillicrap, T. Harley, D. Silver, and K. Kavukcuoglu, "Asynchronous methods for deep reinforcement learning," in *International Conference on Machine Learning*, pp. 1928–1937, 2016.
- [51] D. Silver, G. Lever, N. Heess, T. Degris, D. Wierstra, and M. Riedmiller, "Deterministic policy gradient algorithms," in *International Conference on Machine Learning*, pp. 387–395, 2014.
- [52] H. Geering, G. Dondi, F. Herzog, and S. Keel, "Stochastic systems," *Course script*, 2011.
- [53] S. Ioffe and C. Szegedy, "Batch normalization: Accelerating deep network training by reducing internal covariate shift," in *International Conference on Machine Learning*, pp. 448–456, 2015.
- [54] J. L. Ba, J. R. Kiros, and G. E. Hinton, "Layer normalization," *arXiv preprint arXiv:1607.06450*, 2016.
- [55] D. Q. Mayne, J. B. Rawlings, C. V. Rao, and P. O. Scokaert, "Constrained model predictive control: Stability and optimality," *Automatica*, vol. 36, no. 6, pp. 789–814, 2000.
- [56] R. Tedrake, I. R. Manchester, M. Tobenkin, and J. W. Roberts, "LQR-trees: Feedback motion planning via sums-of-squares verification," *International Journal of Robotics Research*, vol. 29, no. 8, pp. 1038–1052, 2010.